1981

KKR calculation of the electronic structure of cubic WO3 and NaWO3

Lawrence Kopp
Iowa State University

KOPP, LAWRENCE

KKR CALCULATION OF THE ELECTRONIC STRUCTURE OF CUBIC TUNGSTEN-TRIOXIDE AND SODIUM-TUNGSTEN-TRIOXIDE

Iowa State University PH.D. 1981

KKR calculation of the electronic structure of cubic WO_3 and $NaWO_3$

by

Lawrence Kopp

A Dissertation Submitted to the
Graduate Faculty in Partial Fulfillment of the
Requirements for the Degree of
DOCTOR OF PHILOSOPHY

Department: Chemistry
Major: Physical Chemistry

Approved:

Signature was redacted for privacy.

In Charge of Major Work

Signature was redacted for privacy.

For the Major Department

Signature was redacted for privacy.

For the Graduate College

Iowa State University
Ames, Iowa
1981

TABLE OF CONTENTS

LIST OF FIGURES

LIST OF TABLES

CHAPTER I. INTRODUCTION

The transition metal oxides that crystallize as perovskites form a family of isostructural compounds remarkable for the profusion of intriguing properties they display. $SrTiO_3$ is an insulator which when properly doped becomes a superconductor, and its cubic-to-tetragonal structural transformation is the classical example of a displacive phase transition. $BaTiO_3$ is an insulator which at sufficiently low temperature becomes ferroelectric. $LaFeO_3$ is an antiferromagnetic insulator, $GdCoO_3$ and $LaRhO_3$ are semiconductors, and $LaTiO_3$ and $LaNiO_3$ are metallic.

A survey of the more than fifty known members of this family (not counting all the ones with rare-earth elements) has been made by Goodenough (1). His concern was to correlate the change from collective to localized d electron behavior with the row in the periodic table, the formal charge, and the maximum unpaired spin of the transition metal atom. In making this correlation he introduced a phenomenological parameter b, a measure of the strength of the interaction between the d orbitals of the transition metal atom and the orbitals of its nearest neighbors. Those oxides with a value for b greater than the critical value b_c have collective electronic states, while those with a value smaller than b_c have localized electronic states. He then

divided the metallic oxides into two classes according to the origin of their large value for b. Those with strong interactions directly between transition metal atoms, due to the short distance between them, belong to Class I, and those with strong interactions between the transition metal and oxygen atoms, due to large covalent mixing of the metal d and oxygen p orbitals, belong to Class II. Goodenough's suggestion that metallic conductivity in oxides could come from considerable oxygen covalency ran counter to the then prevailing ionic ideas about oxides that were consonant with crystal field theory. Cubic sodium tungsten bronze is one of the Class II oxides.

The tungsten bronzes add to the diversity of the transition metal oxides the dimension of nonstoichiometry. The opportunity they provide to measure or predict properties as a function of composition has made them model systems for study of the solid state. . The sodium tungsten bronzes exhibit a continuous sequence of phases that covers the entire composition range from 0 to 1 sodium atom per unit cell. They have the widest range over which the cubic phase is stable, and this range can be increased by more than a half when metastable crystals with cubic symmetry are included. Tungsten trioxide is monoclinic, and as sodium is added the crystalline symmetry becomes higher, suggesting that the presence of sodium stabilizes the cubic structure. At high

sodium concentrations the conductivity is comparable to that of copper, but the dependence of transport properties on composition cannot be explained by the free-electron approximation. There is a metal-semiconductor transition, and this transition is accompanied by an enhancement of the critical temperature for superconductivity. These properties, taken from among the experimental results that are discussed more fully in the next chapter, are some of the reasons why the sodium tungsten bronzes have been of interest.

Explanation of the metallic properties of the sodium tungsten bronzes has provoked considerable controversy. The main point of contention has concerned which atomic orbitals constitute the conduction band. At least five models have been proposed. These have involved the tungsten 6s states (2), sodium 3p states (3), tungsten 5d (t_{2g}) states (4), sodium states (5), and a covalent admixture of oxygen $2p_{\pi}$ and tungsten 5d (t_{2g}) states (6) in the conduction process.

The last model was proposed by Goodenough (6), who constructed a qualitative energy band scheme applicable to the cubic tungsten bronzes. The method he used was the one used to construct the orbital correlation diagrams of molecular orbital theory. In taking this approach, the energy bands of a crystal are thought of as if they originated from the discrete levels of a molecular cluster. This cluster has the full point group symmetry of the crystal considered,

and is taken to be the constituent element of the crystal's structure. The interaction between those clusters that compose a crystal breaks the degeneracy of their energy levels and spreads them out to form bands. A qualitative band structure for a cubic tungsten bronze crystal can then be inferred from the electronic structure of an octahedral WO_6 molecule.

Features of the electronic structures of the cubic tungsten bronzes have been inferred from these qualitative considerations of Goodenough (6), the tight-binding models of Honig et al. (7), and the ReO_3, $SrTiO_3$, $KTaO_3$, and $KMoO_3$ band calculations of Mattheiss (8-10). Questions remain concerning the details of these band structures, the applicability of the rigid band model when $x \ll 1$, and the participation of the metal atom added to the WO_3 lattice in chemical bonding and physical properties.

To address these questions directly and to help put aside some further speculation, two band structures were calculated at the outset of this study. These were for the two cubic crystals which would, in the absence of structural transformation, lie at each end of the concentration range for the sodium tungsten bronzes: $\square WO_3$ and $NaWO_3$ ($\square$ denotes a vacancy at a Na site). Differences between the results of these two calculations were expected to indicate those features of the electronic structure of cubic Na_xWO_3 which

are sensitive to changes in Na concentration. A third band structure was calculated, one for WO_3 which did not give the vacancies special treatment, in order to determine the influence of the interstitial potential on the band structure. From the energy bands of $NaWO_3$ the density of states and Fermi surface were calculated, and from the wavefunction character of the electronic states were calculated the s, p, and d contributions from each atomic site to the $NaWO_3$ density of states. In making an angular momentum decomposition of the density of states, the calculations have been carried through to the first point of contact between the physics and the chemistry of sodium tungsten bronze. The calculations performed are complete in that they begin at first principles and end at comparison with experimental results. The calculations themselves, their interpretation, and their comparison with experimental data are the outcomes of this study.

CHAPTER II. A REVIEW OF EXPERIMENTAL RESULTS

Bronzes (11) are nonstoichiometric, ternary metal oxides with the chemical formula $M_xT_yO_z$. T is a transition element, T_yO_z is its highest binary oxide, and M is another metallic element whose concentration x may vary over a range that falls within the limits x=0 and x=1. These compounds characteristically pass through a sequence of solid phases as x changes, and these phases may be homogeneous over definite and sometimes wide ranges of M concentrations. They often appear intensely colored, possess metallic lustre as crystals, are very inert chemically, and may exhibit high conductivity. Bronzes can be prepared by vapor-phase reaction, solid-state reaction, or electrolytic reduction. By using electrolysis, large single crystals can be grown.

The tungsten bronzes, M_xWO_3, have been studied extensively (12). Those that have received the most attention have been the alkali tungsten bronzes, especially those with sodium. Sodium tungsten bronze was discovered in 1824 by Woehler (13,14), who noted the formation of golden yellow crystals with a metallic appearance in passing dry hydrogen over heated acid sodium tungstate. Over a century after its first preparation, Haegg (15,16) found that all sodium tungsten bronzes having cubic symmetry fall under the formula Na_xWO_3, where x can vary from about 1 down to about

0.3. The bronzes acquired their name, given to them by Phillip and Schwebel (17), from the deep bronze color of $Na_{0.8}WO_3$. Shanks (18) has described the phases of sodium tungsten bronze obtained by fused salt electrolysis as a function of the temperature and composition of a melt of Na_2WO_4 and WO_3.

Regardless of their symmetry, the phases of all the tungsten bronzes have one common structural feature: they are all an array of WO_6 octahedra linked together at their corners (19). The connections between octahedra in the different phases may leave open trigonal, tetragonal, pentagonal, or hexagonal interstitial sites. All but the trigonal sites may be large enough to accommodate an alkali or other metal atom. Which types of interstitial sites are present, and how many of each type are occupied by a particular metal atom, distinguishes one tungsten bronze from another. WO_3 has a crystal structure composed of octahedra sharing corners just as do its bronzes. A tungsten bronze may then be considered to come from a form of WO_3 whose higher symmetry has been stabilized by the presence of some other metal atoms.

Among the tungsten bronzes, those of sodium seem to be the only ones that form a continuous sequence of phases covering the full range of composition, $0<x<1$. As the sodium concentration decreases, Na_xWO_3 undergoes transitions

that lower its symmetry from cubic (15,16,20-23) to tetragonal (24-27) to orthorhombic (28) to monoclinic (28). When the sodium content is very low, Na_xWO_3 is just lightly doped WO_3, which is itself monoclinic (29). The ranges over which these phases are homogeneous are roughly $1>x\geq0.5$ for the cubic phase, $0.5>x\geq0.2$ for one tetragonal phase (T1), $0.2>x\geq0.06$ for a second tetragonal phase (T2), and $0.06>x$ for the orthorhombic and monoclinic phases. Recent crystal structure determinations of $Na_{0.33}WO_3$ and $Na_{0.48}WO_3$ (24) have shown that the T1 phase actually comprises two different tetragonal space groups. A temperature *versus* composition phase diagram has been constructed for this system by Ribnick *et al*. (28).

One reason Na_xWO_3 is the most studied tungsten bronze is that it has the largest cubic phase region. This region has been extended down to sodium concentrations as low as $x = 0.22$ by diffusing out sodium from a cubic crystal at high temperature and then cooling rapidly (30-34). The metastability of the cubic phase for such low values of x is not too surprising in view of the radical atomic rearrangement needed to transform from the cubic to the T1 structure. Also, the cubic and T2 structures are quite similar, differing most noticeably in the displacement of the tungsten atoms from their cubic positions in the tetragonal phase.

There appears to be a linear relation between the x values and lattice constants of a cubic tungsten bronze (35,36). Measurement of the lattice parameter is often used to find the composition of a cubic M_xWO_3 crystal. Na_xWO_3 is actually cubic for $x \geq 0.5$ only at temperatures above ~400K. At lower temperatures a very small tetragonal distortion has been observed using NMR techniques (37) that has not been detected using X-ray or neutron diffraction.

A partial ordering of the sodium atoms occurs in $Na_{0.75}WO_3$ (21). In this ordered structure the lattice constant is doubled and the simple cubic sublattice of sodium sites has vacancies at the body-centered cubic lattice points of the new unit cell. Anomalies appear in the x-dependence of the resistivity, the Hall coefficient, and the Seebeck coefficient in the vicinity of this sodium ordering (38).

A connection between the cubic structure and the metallic behavior of a tungsten bronze is suggested by the observation (30) that, for any metal atom M, there seems to be no known M_xWO_3 crystal which becomes cubic without also becoming metallic. The high electrical conductivity of tungsten bronzes with a high value of x for the oxidation state of M has drawn much of the attention given to these materials. Pure WO_3 is an insulator (39,40). At 300K the conductivity of $Na_{0.88}WO_3$ is 0.64×10^5 $(\Omega\text{-cm})^{-1}$ (38), and

rises rapidly as x increases. This approaches the conductivity of copper, which is 5.88×10^5 $(\Omega\text{-cm})^{-1}$ at 295K (41).

Many measurements have been made of the electronic transport properties of the sodium tungsten bronzes (30,31, 34,38,42-48). These include resistivity, Hall coefficient, and Seebeck coefficient data taken on samples with sodium concentrations that cover the entire cubic phase region, and taken at temperatures from 4.2 to 300K. The conductivities of Li_xWO_3, Na_xWO_3, and K_xWO_3 show practically no dependence upon either the alkali atom or the crystal structure, and vary with x in a manner indicative of a metal-nonmetal transition at $x \sim 0.2$ (43,49).

The Hall coefficients of Na_xWO_3 are independent of temperature from liquid helium to room temperature. For crystals homogeneous in electrical resistivity, the Hall coefficient, R, leads to an effective number of conduction electrons, $n^* = 1/Re$, that is greater than the number of sodium atoms per unit volume. The actual number of conduction electrons is expected to be less than the effective number determined from the Hall coefficient when the Fermi surface is not spherical (38). The diffusion contribution to the Seebeck coefficient is not proportional to $x^{-2/3}$, and the lattice contribution to the Seebeck coefficient exhibits variations with x consistent with a nonspherical Fermi surface for Na_xWO_3 (42). These results have been

interpreted, under the assumption that each sodium atom contributes one electron to the conduction band, as evidence that the free-electron approximation does not provide a satisfactory explanation of the electronic properties of the sodium tungsten bronzes.

The heat capacity (32,50-52) and magnetic susceptibility (32,53-56) results for the cubic sodium tungsten bronzes concur in the conclusion that the conduction electrons do not conform to a free-electron model. Both the electronic contribution to the heat capacity and the contribution to the susceptibility of the conduction electrons due to Pauli spin paramagnetism are proportional to the density of states (to a first approximation). The density of states at the Fermi energy deduced from the heat capacity and magnetic susceptibility data depends linearly on the sodium concentration x, and has a nearly zero intercept. An $x^{1/3}$, not an x, dependence follows from the free-electron model. This indicates that the density of states increases faster with energy than the rate of a parabolic, nearly free-electron band (for which the density of states is proportional to $E^{1/2}$). The weak paramagnetism of cubic Na_xWO_3 was found to be independent of temperature from 70 to 300K (53).

The metallic behavior of the sodium tungsten bronzes that is reflected in their electrical, magnetic, and thermal properties might well be expected to evidence itself in a

relatively large, positive (Knight) shift of the ^{23}Na nuclear magnetic resonance (NMR). A strong paramagnetic shift is characteristic of the interaction of the nuclei with the conduction electrons in ordinary metals (57). However, NMR measurements of the ^{23}Na resonance in several sodium tungsten bronze crystals detected very small (nearly zero), diamagnetic shifts with respect to the ^{23}Na resonance in aqueous NaCl (58). This result indicates that, despite the fact that the conduction electrons come from the sodium atoms, there must be little, if any, sodium s character in the electronic states near the Fermi level.

Sodium tungsten bronze has been the subject of several NMR studies (33,37,58-60). Both the ^{23}Na and ^{183}W resonances have been observed. For both these nuclei in cubic Na_xWO_3 the relaxation rate $(T_1T)^{-1}$ is proportional to x^2 (T_1 is the nuclear spin-lattice relaxation time and T is the temperature) (33). According to a one-electron theory for a homogeneous metal, $(T_1T)^{-1}$ is also proportional to the square of the density of states at the Fermi energy. Taken together, these results indicate that the density of states is proportional to x, in agreement with the heat capacity and magnetic susceptibility results, provided that the cubic sodium tungsten bronzes are homogeneous metals.

The ability to control the number of conduction electrons through changes of composition has made the study

of superconducting properties in the tungsten bronze system of particular interest. The first report of superconductivity in this system was made by Raub et al. (61). They observed a superconducting transition temperature of about 0.57K in the T1 phase of sodium tungsten bronze. A dramatic increase in this critical temperature, T_c, with decreasing sodium concentration, x, has been observed by Shanks (62) as the composition at which the transition occurs from the T1 to the T2 phase is approached. As the x-value decreases, the transition temperatures increase exponentially from a $T_c \sim 0.7K$ at $x \sim 0.4$ to a $T_c \sim 3K$ at $x \sim 0.2$. The fact that this enhancement of T_c is associated with both a phase transition and a metal-semiconductor transition suggested the possibility that a soft mode instability might be influencing the electron-phonon interaction.

Ngai and Silberglitt (63) studied the effect of lattice instability on superconductivity in sodium tungsten bronze. They proposed a simple model from which they concluded that, to correctly predict the enhancement of T_c very near the transition, phonon-configuration coupling is essential. In this system the simultaneous occurrence of a superconducting and a structural transition is possible because the phonon that assists configurational tunneling between the tetragonal phases softens as a function of composition, not of temperature.

CHAPTER III. UNDERLYING THEORETICAL IDEAS

Bringing the Many-Body Problem to One-Electron Form

Quantum mechanical calculations of the properties of solids begin with the simplification of Schroedinger's equation for a system of perhaps 10^{23} or more nuclei and electrons. The Born-Oppenheimer approximation (64) separates the motion of the electrons from the motion of the nuclei, and leaves a many-body problem for the motion of the electrons in the field of nuclei placed at fixed positions. The Hartree approximation (65-67) replaces the instantaneous interaction between each pair of electrons by an interaction between a single electron and a self-consistent field that simulates the collective effect of all the other electrons. Consideration of the antisymmetry of electronic states to an interchange of the coordinates (space and spin) of any two electrons, leads in the Hartree-Fock approximation (68) to a self-consistent field in which all electrons use all orbitals in a way that agrees with the Pauli exclusion principle (69).

The great lowering of difficulty gained by calling upon these approximations comes with a weakening of the theory, since the neglected interactions do exhibit very interesting observable effects (70). The electron-phonon interaction can enhance the effective electron mass, the electronic specific heat, and the oscillator strength of optical

transitions, and is central to the theory of superconductivity. Electron-electron correlation plays an important part in plasma oscillations in metals, exciton effects in insulators and semiconductors, ferromagnetism in transition metals, and the simultaneous appearance of localized and itinerant properties.

Use of the Born-Oppenheimer and Hartree-Fock approximations bases the calculation of electronic properties on a one-electron (or independent particle) model. Within this model the Hartree-Fock equations afford the "best" set of orbitals (up to an arbitrary unitary transformation). Close approximations to solutions of the Hartree-Fock equations can now be found without extraordinary effort, either numerically or analytically, for all the atoms and for many small molecules, but not for solids. What makes solution of the Hartree-Fock equations so difficult, especially for solids, is the way that they eliminate the self-interaction of the electrons that is implicit in their coulomb terms. The exchange terms serve solely to rid the equations of those impossible encounters in which an electron repels itself (71). They achieve this by associating each orbital with a different potential field. Having to deal with potentials that are different for each orbital considerably complicates solution of the equations.

Not only are the Hartree-Fock equations intractable for solids, but their solutions are suspect, since their exact solution for a free-electron gas predicts the vanishing of the density of states at the Fermi energy. This conflicts with the well-known free-electron-like behavior of the simple metals, for which a density of states proportional to the square root of the Fermi energy leads to good agreement with measurements of the heat capacity and paramagnetic susceptibility of the conduction electrons. This discrepancy comes from the dependence of the exchange term in the Hartree-Fock equations on the orbital considered. For a free-electron gas this orbital dependence of exchange proves to be nearly cancelled by a similar dependence of the long-range correlation among the electrons (72). An inability to describe long-range correlation is inherent in a Hartree-Fock wavefunction, since it introduces exchange terms which are always positive (71).

Slater's Statistical Exchange Approximation

To avoid both the difficulties in solving the Hartree-Fock equations, and the suspected inadequacy of their solutions for solids, resort is often taken to Slater's statistical exchange (or $X\alpha$, or $\rho^{1/3}$) approximation (73-75). The heuristic argument that recommends this approximation rests upon an interpretation of exchange much like the idea of the

Fermi hole (76-78). Each electron is surrounded by a region from which a probability density equal to that for one electron is excluded. Then, in a system with N electrons, each electron will interact, as it should, only with the N-1 other electrons (not with N, as is the case for the pair density that determines the coulomb potential).

Slater's interpretation of exchange refers, not to the usual form of this term in the Hartree-Fock equations,

$$V_{XHFi}(1)\phi_i(1) = \left[-\sum_j n_j \int dv_2 \phi_j^*(2)\phi_i(2) \frac{1}{r_{12}}\right]\phi_j(1), \qquad (1)$$

but to the equivalent form,

$$V_{XHFi}(1)\phi_i(1) = \left[-\int dv_2 \sum_j n_j \frac{\phi_i^*(1)\phi_j(1)\phi_j^*(2)\phi_i(2)}{\phi_i^*(1)\phi_i(1)} \times \frac{1}{r_{12}}\right]\phi_i(1). \qquad (2)$$

Here (using atomic units, but with energies in rydbergs) the orbitals, ϕ_i and ϕ_j, themselves solutions of the Hartree-Fock equations, are occupied by two electrons, 1 and 2, that are a distance r_{12} apart. The number of electrons in orbital ϕ_j is n_j, where $n_j = 1$ if ϕ_j is occupied and $n_j = 0$ if it is not. The equivalent expression (Eq. 2) restores each Hartree-Fock equation to the more familiar form of a one-electron Schroedinger equation, in which the wavefunction of an

orbital is simply multiplied by the potential of the motion in that orbital.

The exchange potential of orbital i, V_{XHFi}, is construed as if it were for the classical electrostatic interaction between an electron and the exchange charge density

$$\rho_{XHFi}(1,2) = \sum_j n_j \frac{\phi_i^*(1)\phi_j(1)\phi_j^*(2)\phi_i(2)}{\phi_i^*(1)\phi_i(1)} \quad . \tag{3}$$

This exchange charge density has two noteworthy characteristics. When the coordinates of electrons 1 and 2 are the same, ρ_{XHFi} equals the total charge density at that point:

$$\rho_{XHFi}(1,1) = \sum_j n_j \, \phi_j^*(1)\phi_j(1) = \rho(1) \quad . \tag{4}$$

When integrated over the coordinates of electron 2, ρ_{XHFi} is seen to be a distribution of one electronic charge (assuming orbital i is occupied):

$$\begin{aligned} \int dv_2 \, \rho_{XHFi}(1,2) &= \sum_j n_j \frac{\phi_i^*(1)\phi_j(1)}{\phi_i^*(1)\phi_i(1)} \int dv_2 \, \phi_j^*(2)\phi_i(2) \\ &= \sum_j n_j \frac{\phi_i^*(1)\phi_j(1)}{\phi_i^*(1)\phi_i(1)} \delta_{ij} \\ &= n_i = 1 \quad . \end{aligned} \tag{5}$$

These two characteristics, taken together, indicate that each exchange charge density is concentrated about the

position of electron 1, and is carried along with this electron. An electron in a crystal, no matter where it happens to be, then always finds itself in the field of an atom minus one electron and other atoms that are all neutral.

Since the exchange charge densities of the occupied orbitals all equal $\rho(1)$ whenever the positions of electrons 1 and 2 are the same, and since they all integrate over space to the charge of one electron, Slater argues that they must not differ much from one another. This provides a rationale for use of a weighted average of the exchange charge densities of the different occupied orbitals. Replacement of the exchange charges in the Hartree-Fock equations with their weighted average makes all the orbitals solutions for a single potential field.

The averaged Hartree-Fock exchange potential is in general not much easier to use than the original, individual exchange potentials for each orbital. For a free-electron gas, however, this potential can be calculated exactly:

$$\left[V_{XHFi}(1)\right]_{av} = -6\left[\frac{3}{8\pi}\,\rho(1)\right]^{1/3} . \qquad (6)$$

At this point, Slater, by a grand act of intuition, suggests that a bona fide approximation to the Hartree-Fock exchange potential may be made by using instead the potential of Eq. 6 where $\rho(1)$ is the local charge density as given in

Eq. 4. The impulse behind this proposition comes from Eqs. 3 and 4, and from a simple dimensional argument concerning the electrostatic potential at the center of the Fermi hole. These lend support to the idea that the exchange potential depends primarily upon the charge density, and rather little upon other things, regardless of whether or not the system is a free-electron gas.

Use of a local function of the charge density in place of the nonlocal exchange potential of the Hartree-Fock equations greatly simplifies solution of the one-electron problem. In calculations of the electronic states of crystals, the Slater exchange approximation automatically preserves the correct periodicity. Although the Hartree-Fock method is to be preferred as far as energies are concerned, the Hartree-Fock-Slater method has distinct advantages when dissociation, or the application of Fermi statistics, is considered.

The Korringa-Kohn-Rostoker (KKR) Method

The KKR method is presented in five standard papers (79-83). The theory was developed independently by Korringa (79), from a multiple scattering point of view, and by Kohn and Rostoker (80), from a Green's function approach. Segall (81) extended the theory to crystals with more than one atom per unit cell, and Ham and Segall (82) emphasized the need

to use the full Ewald summation procedure in order to obtain good convergence in the evaluation of the expansion coefficients of the Green's function. Myron (84) has presented the final formulas of the KKR method for several atoms per unit cell, including Ewald's method. The purpose of the following presentation is to give a more coherent and elementary treatment to the theory that stresses important points left unstated in the terse standard references.

The time-independent Schroedinger equation determines the stationary states of a system - the states for which a wavefunction, ψ, has a definite value of energy, E. Solving for ψ and E is so difficult a problem that simplified models must be introduced for all but the simplest physical systems. Such models are made (in a manner that may or may not be self-consistent) by assuming certain forms for the wavefunction and for the potential term in the Hamiltonian. An approximate method for solving Schroedinger's equation may proceed from one of these models in several markedly different ways.

The form chosen for the wavefunction may determine the potential, or the form chosen for the potential may determine the wavefunction. The wavefunction may be determined by minimizing the energy, or the energy may be determined by boundary conditions on the wavefunction. Values for the energy may or may not be found by solving for the eigenvalues

of a hermitian operator or matrix. These differences have been mentioned because their recognition beforehand is helpful in coming to an appreciation of the KKR method. To make them plain, consider the following two examples.

In the independent particle model, the wavefunction ψ that represents a closed-shell ground state has the form of a single antisymmetrized product of spin orbitals, ϕ. This functional form may be used directly to estimate the energy as the expectation value of the Hamiltonian, $\langle H \rangle$. $\langle H \rangle$ then becomes a sum of kinetic energy, nuclear attraction, coulomb, and exchange integrals, each of which is an energy contribution from one of the ϕ's to the total energy. Since the interelectronic potential depends upon the ϕ's, the wavefunction chosen here determines the potential. Parameters present in this form of wavefunction may now be varied so as to minimize the total energy in accordance with the variational theorem. Setting the variation of $\langle H \rangle$ equal to zero, with the ϕ's themselves as the adjustable parameters (and under the constraint that the ϕ's be orthonormal) leads to a set of equations that a best set of ϕ's must satisfy - the Hartree-Fock equations. In these equations the ϕ's are all eigenfunctions of the same hermitian operator, and the eigenvalues are the orbital energies. Since the Hartree-Fock equations are themselves very difficult to solve, the ϕ's are usually approximated by an expansion in a set of basis

functions (often Slater- or gaussian-type orbitals). $\langle H \rangle$ is then minimized with respect to the coefficients. This reduces the problem to one of solving a generalized eigenvalue equation involving hermitian matrices. The matrix elements are integrals of the same hermitian operator between each pair of basis functions. (The difficulty of evaluating these integrals often leads to further simplifications, and to correspondingly less and less rigorous models.) Each matrix element has an interpretation as a kind of interaction energy. The eigenvalues of this matrix are the orbital energies, and the eigenvectors are the expansion coefficients of the ϕ's.

This example is just the approximate method for solving Schroedinger's equation most familiar to those who have studied quantum chemistry (molecular orbital theory is based upon it). What characterizes this approach is the central role the energy plays: the magnitude of E determines the quality of ψ (the lower E, the better ψ). Emphasis on the energy agrees well with the preoccupation in chemistry with questions of chemical bonding and stability.

The KKR method is a development in solid state physics, and differs in almost all respects from the foregoing approach. By way of contrast to what is common practice in molecular orbital calculations, an approach akin to the KKR method is taken in the second example.

Consider a model that simplifies a physical system down to the problem of the motion of a particle in a spherically symmetric potential. Such a model, with a potential proportional to the square of the radius, is of interest in the study of some nuclear properties. A potential inversely proportional to the radius, as is the potential of a coulomb field, might make this a model of the hydrogen atom, or of an ion with but one electron (like Be^{+++}). Since the Hamiltonian, expressed in spherical coordinates (r,θ,ϕ), with a potential that depends only upon r, commutes with the operators for the square of the angular momentum and the z-component of the angular momentum, the wavefunctions of the stationary states can be simultaneous eigenfunctions of all three operators. The wavefunctions can then be written as the product of an imaginary spherical harmonic times a radial function that depends upon the potential, the energy, and the total angular momentum. Here the appropriate potential determines the form of the wavefunction. The radial functions satisfy a differential equation, and may be found by numerical integration. Solutions of this radial equation exist for all values of the energy, but boundary conditions on the wavefunction may allow only certain solutions and energy values. Requiring the wavefunction to be finite at the origin, and zero at infinity, leads to the energy levels of the hydrogen atom.

The relation of this example to the KKR method arises from the use in the KKR method of spherically symmetric potentials about all the atomic sites in a crystal, and from the emphasis placed upon the wavefunction and its determination by the appropriate boundary conditions. Of course, in a crystal the wavefunction about an atomic site need no longer satisfy the boundary conditions for a free atom. And although the potential about each site has spherical symmetry (locally), the wavefunction must nonetheless meet the demands of an effective crystalline potential that has the full space group symmetry.

An integral form of Schroedinger's equation: the Green's function approach

Emphasis upon the wavefunction is made manifest in the development of the theory at the outset. The KKR method departs from the accustomed stratagems for solving Schroedinger's equation by dealing with this equation, not in its familiar form as a homogeneous, second-order, linear, partial differential equation,

$$(-\nabla^2 + V(\underline{r}) - E)\psi(\underline{r}) = 0, \tag{7}$$

but in its equivalent, though less well-known, form as a homogeneous integral equation,

$$\psi(\underline{r}) = \int d^3\underline{r}'g(\underline{r},\underline{r}')V(\underline{r}')\psi(\underline{r}'). \tag{8}$$

The Green's function, $g(\underline{r},\underline{r}')$, solves the differential equation

$$(\nabla^2 + E)g(\underline{r},\underline{r}') = \delta(\underline{r}-\underline{r}'), \tag{9}$$

where $\delta(\underline{r}-\underline{r}')$ is the delta function.

The equivalence of the differential and integral forms of Schroedinger's equation is easily verified by first operating on both sides of Eq. 8 with $(\nabla^2 + E)$, and then by using Eq. 9 to show that the right-hand-side becomes $V(\underline{r})\psi(\underline{r})$. (Note that $(\nabla^2 + E)$ may be brought inside the integral, because it operates on $\underline{r}$ while the integration is over $\underline{r}'$.)

The Green's function, or free-particle propagator, that solves Eq. 9 can be expressed explicitly as

$$g(\underline{r},\underline{r}') = g(\underline{r}-\underline{r}') = -\frac{1}{4\pi}\frac{e^{i\kappa|\underline{r}-\underline{r}'|}}{|\underline{r}-\underline{r}'|}, \text{ where } \kappa^2 = E. \tag{10}$$

Note that in Eq. 8, the energy E, upon which the Green's function depends, is the eigenenergy of the Schroedinger equation, and that for particular boundary conditions, the integral equation, just like the differential equation, has solutions only for certain values of E.

Equivalence of the integral equation to a variational principle

When the exact solution to an equation is unknown (as is almost always true of the solution to Schroedinger's equation), physical intuition, theoretical arguments, or hard experience may suggest that the solution sought has a form somewhat

like one that is attainable with a specific trial function. Among those methods for obtaining an approximate solution that use trial functions, and that take the general approach known as the method of weighted residuals, the variational method possesses several advantages (85,86). Of these methods, only the variational method guarantees real values when used for finding approximate solutions to eigenvalue problems. Besides providing an approximate solution, the variational method provides an accurate value for some characteristic quantity - the functional whose variation is considered. When $\langle H \rangle$ is varied, subject to the normalization of ψ, an accurate value is found for E. As is well-known, accuracy to only first-order in the approximate solution results in accuracy to second-order in the value of the functional. Since it is usually possible for errors to cancel, an accurate functional may come from an inaccurate function. Nonetheless, the value of the variational method lies in part in that the value of the functional provides a (more or less sensitive) criterion with which to measure how good a particular approximate solution happens to be.

In essence the variational method seeks to find a functional, Λ, whose stationary values are determined by the equation whose solution is sought. Or put slightly differently, the function that satisfies the variational principle, $\delta\Lambda = 0$, is the very function that solves the

equation that has yet to be solved. The functional whose stationary values occur for solutions to the (differential) Schroedinger equation satisfied by both ψ and ψ^* is

$$\Lambda = \tfrac{1}{2}\{\int d\tau \psi^*(H-E)\psi + \int d\tau \psi(H-E)\psi^*\} \tag{11}$$

(an expression for Λ symmetric in ψ and ψ^*). The first variation of Λ (considering ψ and ψ^* to be independent) is then

$$\delta\Lambda = \tfrac{1}{2}\{\int d\tau [\delta\psi^*(H-E)\psi + \psi^*(H-E)\delta\psi] + \int d\tau [\delta\psi(H-E)\psi^* + \psi(H-E)\delta\psi^*]\},$$

which may be rewritten (adding and subtracting integrals involving ∇^2) as

$$\delta\Lambda = \int d\tau \delta\psi^*(H-E)\psi + \tfrac{1}{2}\int d\tau [\delta\psi^*\nabla^2\psi - \psi\nabla^2\delta\psi^*] + \int d\tau \delta\psi(H-E)\psi^* + \tfrac{1}{2}\int d\tau [\delta\psi\nabla^2\psi^* - \psi^*\nabla^2\delta\psi]. \tag{12}$$

This last equation makes plain that, when ψ and ψ^* are solutions to Schroedinger's equation, Λ is stationary, not for arbitrary variations of ψ and ψ^*, but for those variations for which the second and fourth terms also are zero.

These two seemingly troublesome terms have an interpretation based upon the time-derivative of the probability density, $\rho = \psi^*\psi$. If ψ and ψ^* are exact solutions to time-dependent Schroedinger equations, then

$$\frac{\partial}{\partial t}\rho = \frac{i}{\hbar}(\psi^*\nabla^2\psi - \psi\nabla^2\psi^*).$$

The second term is the variation of $-\frac{1}{2}i\hbar\partial/\partial t\int d\tau\rho$ with respect to ψ^*, and the fourth term is the variation of $\frac{1}{2}i\hbar\partial/\partial t\int d\tau\rho$ with respect to ψ. These terms are zero if the probability density is conserved (as it must be for any closed physical system). By using Green's theorem to transform each volume integral into a surface integral, both of these terms can be interpreted as a boundary condition. They are zero when the flux into or out of a system is zero. For a bound state of an atom or molecule, they are zero because, everywhere on the boundary at infinity, the wavefunction must be zero. For a propagating state of an infinite crystal, they are zero when the wavefunction has the correct translational symmetry (when the wavefunction is a Bloch function). Then the contributions from conjugate points on the surface of a unit cell exactly cancel (as many electrons enter a unit cell as leave it). Furthermore, these boundary conditions on ψ and ψ^* must equal zero for the Hamiltonian to be hermitian (as may be shown by shifting H, say, from ψ to ψ^* using integration by parts). Because of this, care must be taken not to use the prior knowledge that the Hamiltonian must be hermitian in carrying through the manipulations that lead to Eq. 12. When the boundary terms in this equation equal zero, solving the variational problem for the functional

set forth in Eq. 11 is completely equivalent to solving Schroedinger's equation.

The variational principle that is equivalent to the differential form of Schroedinger's equation (discussed as an example up to this point) has one further advantage of its own. Not only does it provide an estimate of the energy, but it provides one that is an upper or lower bound to the true value of the energy. This principle reduces to the minimization of $\langle H \rangle$ in order to find the "best" ground state wavefunction attainable with a specific trial function (if this function is already normalized). As will be shown next, the variational principle that is equivalent to the integral form of Schroedinger's equation does not share this advantage.

The functional whose stationary values occur for solutions to the integral equation is

$$\Lambda = \int d^3\underline{r}\psi^*(\underline{r})V(\underline{r})\psi(\underline{r}) - \int d^3\underline{r}\int d^3\underline{r}'\psi^*(\underline{r})V(\underline{r})g(\underline{r},\underline{r}')V(\underline{r}')\psi(\underline{r}') \qquad (13)$$

(an expression, like that for Λ in Eq. 11, symmetric in ψ and ψ^*). The equivalence of the variational principle, $\delta\Lambda = 0$, to Eq. 8 is not difficult to prove. What is noteworthy is that, unlike in Eq. 12, no boundary terms occur (the integrands involve no differential operators). Λ is stationary for arbitrary variations of ψ and ψ^* - even for

those that violate the conditions which the true solution must satisfy.

The relationship between Λ in Eq. 11 and Λ in Eq. 13 is revealed by taking the following steps. Letting

$$\phi(\underline{r}) = \int d^3\underline{r}' g(\underline{r},\underline{r}')V(\underline{r}')\psi(\underline{r}'), \tag{14}$$

and using Eq. 9, Eq. 13 becomes

$$\begin{aligned}\Lambda &= \int d^3\underline{r}\psi^*(\underline{r})\int d^3\underline{r}'\delta(\underline{r}-\underline{r}')V(\underline{r}')\psi(\underline{r}') - \int d^3\underline{r}\psi^*(\underline{r})V(\underline{r})\phi(\underline{r}) \\ &= \int d^3\underline{r}\psi^*(\underline{r})\int d^3\underline{r}'(\nabla^2+E)g(\underline{r},\underline{r}')V(\underline{r}')\psi(\underline{r}') \\ &\qquad - \int d^3\underline{r}\psi^*(\underline{r})V(\underline{r})\phi(\underline{r}) \\ &= \int d^3\underline{r}[\psi^*(\underline{r})(\nabla^2+E)\phi(\underline{r}) - \psi^*(\underline{r})V(\underline{r})\phi(\underline{r})] \\ &= -\int d\tau\psi^*(H-E)\phi. \end{aligned} \tag{15}$$

If the boundary conditions are satisfied so that H will be hermitian, the two variational functionals reduce to one another when ϕ equals ψ. They are the same only for the solutions to the integral Schroedinger equation, only when Eq. 14 becomes Eq. 8. For a trial wavefunction, the variational functional used in the KKR method is not simply related to the expectation value of the Hamiltonian, and will not provide an energy which is a bound to the true value of the energy.

An interpretation of Λ, which brings out the significance of this functional as a measure of the quality of an

approximate solution, follows (using Eq. 14) from expression of Λ as an expectation value:

$$\Lambda = \int d\tau \psi^* V\psi - \int d\tau \psi^* V\phi = \langle V(\psi-\phi)/\psi \rangle .$$

If ψ were the exact solution to Schroedinger's equation, ϕ would be identical to ψ (Eq. 14 would become Eq. 8), and Λ would equal zero. When ψ is some trial function, $\phi \neq \psi$, and Λ represents an average residual potential energy due to the difference between them. Alternatively, and more in the spirit of the KKR method, due to an emphasis on the wavefunction rather than on the energy, Λ may be interpreted as an average error in ϕ relative to ψ that is weighted by the potential, V. This weighting is important if the variational principle is to produce an approximate solution with an acceptable energy. The energy is most sensitive to those errors in the wavefunction present where the potential is deepest. As a consequence the variational process may be expected to do whatever it can to lessen the errors (or perhaps promote cancellation of the errors) that occur in the regions closer to nuclei, to the detriment of those regions farther away. In the KKR method the variational process attempts to minimize the difference between ϕ and ψ. The "best" ψ is the one which most nearly transforms into itself, as does the exact solution to the integral Schroedinger equation.

Integral Schroedinger equation for a periodic potential

If the stationary states determined by the Schroedinger equation are those for the motion of an electron in the periodic potential of a perfect crystal ($V(\underline{r}) = V(\underline{r}-\underline{r}_s)$, where $\underline{r}_s$ is one of the translation vectors of the crystal lattice), the integral in Eq. 8 can be changed from one over the entire coordinate space to one over the volume of just a single unit cell (87). This may be achieved by a geometrical partitioning of the crystalline potential:

$$V(\underline{r}) = \sum_s v(\underline{r}-\underline{r}_s), \text{ where } v(\underline{r}-\underline{r}_s) = \begin{cases} V(\underline{r}) & \text{inside cell s} \\ 0 & \text{outside} \end{cases}.$$

By substituting this potential into Eq. 8, the integral becomes a sum of contributions from the individual cells:

$$\psi(\underline{r}) = \sum_s \int_{\tau_s} d^3\underline{r}' g(\underline{r}-\underline{r}')v(\underline{r}'-\underline{r}_s)\psi(\underline{r}'),$$

where τ_s is the volume bounded by unit cell s. Changing the variable $\underline{r}'$ to $\underline{r}'+\underline{r}_s$,

$$\psi(\underline{r}) = \int_{\tau} d^3\underline{r}' \sum_s g(\underline{r}-\underline{r}'-\underline{r}_s)v(\underline{r}')\psi(\underline{r}'+\underline{r}_s),$$

and using Bloch's theorem,

$$\psi_{\underline{k}}(\underline{r}'+\underline{r}_s) = e^{i\underline{k}\cdot\underline{r}_s}\,\psi_{\underline{k}}(\underline{r}'),$$

returns the integral Schroedinger equation to its original form,

$$\psi(\underline{r}) = \int_{\tau} d^3\underline{r}' G(\underline{r},\underline{r}')V(\underline{r}')\psi(\underline{r}'), \qquad (16)$$

but with integration over only one unit cell, and with $g(\underline{r},\underline{r}')$ replaced by the complete Green's function,

$$G(\underline{r},\underline{r}') = G(\underline{r}-\underline{r}') = \sum_s g(\underline{r}-\underline{r}'-\underline{r}_s)e^{i\underline{k}\cdot\underline{r}_s}. \qquad (17)$$

G solves the same differential equation as does g (Eq. 9), and Eq. 16 is equivalent to a variational functional like Eq. 13, but with G replacing g.

Transformation of the integral Schroedinger equation to a surface condition

The crystalline wavefunction, $\psi(\underline{r})$, which in Eq. 16 transforms into itself under multiplication by GV and integration over the volume of a unit cell, satisfies an equivalent equation that is a surface condition on the faces of a unit cell. To derive this equation, note that

$$\psi(\underline{r}) = \int_\tau d^3\underline{r}'\psi(\underline{r}')\delta(\underline{r}-\underline{r}'),$$

use this relation to rewrite Eq. 16 as

$$\int_\tau d^3\underline{r}'[\psi(\underline{r}')\delta(\underline{r}-\underline{r}') - G(\underline{r},\underline{r}')V(\underline{r}')\psi(\underline{r}')] = 0,$$

substitute for $\delta(\underline{r}-\underline{r}')$ from Eq. 9 (replacing g with G) and for $V\psi$ from Eq. 7,

$$\int_\tau d^3\underline{r}'[\psi(\underline{r}')\nabla'^2G(\underline{r},\underline{r}') - G(\underline{r},\underline{r}')\nabla'^2\psi(\underline{r}')] = 0,$$

and apply Green's theorem to transform from a volume to a surface integral,

$$\int_{\sigma} d\underline{s}' \cdot [\psi(\underline{r}')\underline{\nabla}' G(\underline{r},\underline{r}') - G(\underline{r},\underline{r}')\underline{\nabla}'\psi(\underline{r}')] = 0. \qquad (18)$$

σ is the surface of a unit cell.

This condition, Eq. 18, is reminiscent of the problem encountered in the cellular method of matching an approximate wavefunction in contiguous cells at the boundary. In the KKR method an approximate ψ will not transform into itself (Eq. 16), but will become instead some ϕ. Eq. 16 then no longer holds true (the leftmost ψ should be ϕ), and the surface integral of Eq. 18 equals a nonzero value that measures the disparity between ψ and ϕ at all points on the boundary of a cell. Variation of Λ (Eq. 13), say, with respect to the expansion coefficients of ψ is here seen to be an attempt to minimize the mismatch between ψ and ϕ over σ. As in the cellular method, solution of Eq. 18 is frustrated by the need to accurately extend the wavefunction out into the corners of a unit cell, and to perform an integration over the surface of a polyhedron as complex as a Wigner-Seitz cell.

Simplifications from use of a muffin-tin (MT) potential

These difficulties do not arise when an approximation to the crystalline potential, $V_{MT}(\underline{r})$, is constructed which is spherically symmetric within a radius R_j of each atomic site j and constant everywhere else. The radii of the regions with spherical symmetry must be chosen so that the

spheres about each atomic site do not overlap. The energy scale may then be chosen so that the constant potential between these spheres, the average of the crystalline potential over this interstitial region, equals zero. This muffin-tin approximation to the potential is best for those crystals with a closely packed structure, where MT spheres can be chosen so that their total volume per unit cell is a large percentage of a cell's volume.

When $V_{MT}(\underline{r})$ replaces $V(\underline{r})$ in Eq. 16, only the volume enclosed by the MT spheres contributes to the integral, since $V_{MT}(\underline{r}) = 0$ everywhere outside them. Eq. 18 then becomes a sum of integrals, each one over the surface of a MT sphere, $\sigma_{j'}$:

$$\sum_{j'} \int_{\sigma_{j'}} ds' [\psi^{j'}(\underline{r}'_{j'}) \frac{\partial}{\partial r'_{j'}} G^{(j,j')}(\underline{r}_j, \underline{r}'_{j'}) - G^{(j,j')}(\underline{r}_j, \underline{r}'_{j'}) \frac{\partial}{\partial r'_{j'}} \psi^{j'}(\underline{r}'_{j'})] = 0. \quad (19)$$

With use of a muffin-tin potential, ψ and G are best represented in spherical coordinates, $\underline{r}_j$ and $\underline{r}'_{j'}$, centered on atomic sites j and j'. In these coordinates the gradient normal to the surface of MT sphere j' is just the partial derivative with respect to the radial component $r'_{j'}$.

The wavefunction inside MT sphere j', $\psi^{j'}$, is a solution to the Schroedinger equation whose potential is the spherical average of the crystalline potential inside this

sphere. The problem of a particle moving in a field with spherical symmetry has as an exact solution an infinite series expansion in spherical harmonics, Y_{LM}:

$$\psi^{j'}(\underline{r}'_{j'}) = \sum_{LM} c^{j'}_{LM} R^{j'}_{L,E}(r'_{j'}) Y_{LM}(\hat{r}'_{j'}), \quad r'_{j'}<R_{j'}. \tag{20}$$

The c's are expansion coefficients to be determined by the surface condition defined by Eq. 19. The R's are energy-dependent solutions to the radial Schroedinger equation:

$$\left[-\frac{1}{r^2}\frac{d}{dr}r^2\frac{d}{dr} + \frac{\ell(\ell+1)}{r^2} + V(r) - E\right]R_{L,E}(r) = 0,$$

where R must be finite at the origin (here the prime on r and the index j' are irrelevant). A further approximation is introduced when, as a practical matter, the series in Eq. 20 is truncated to the first few terms. This truncation affects the accuracy of the desired eigenvalues E. One of the strengths of the KKR method is its very good convergence, as evidenced by the need, ordinarily, to use values of L only up to 2 in order to obtain sufficiently good results.

Now an appropriate explicit expression for G is needed where it enters Eq. 19.

Various expressions for the Green's function

Placing the explicit expression for $g(\underline{r},\underline{r}'+\underline{r}_s)$ (Eq. 10) into Eq. 17 gives the real lattice representation of the complete Green's function:

$$G(\underline{r},\underline{r}') = -\frac{1}{4\pi}\sum_s \frac{e^{i\kappa|\underline{r}-\underline{r}'-\underline{r}_s|}}{|\underline{r}-\underline{r}'-\underline{r}_s|}\, e^{i\underline{k}\cdot\underline{r}_s}, \text{ where } \kappa^2 = E. \qquad (21)$$

A reciprocal lattice representation of $G(\underline{r},\underline{r}')$ can be found by replacing $g(\underline{r}-\underline{r}'-\underline{r}_s)$ in Eq. 17 with its $\underline{k}$-space representation. Such an expression for $g(\underline{r},\underline{r}')$ comes from its expansion in the solutions to the homogeneous boundary value problem, $(\nabla^2 + E)\, f(\underline{r}-\underline{r}') = 0$ (recall that $g(\underline{r}-\underline{r}')$ is a solution to Eq. 9). These solutions are the free-particle eigenfunctions (plane waves),

$$f_{\underline{k}}(\underline{r}-\underline{r}') = \frac{1}{T}\, e^{i\underline{k}\cdot(\underline{r}-\underline{r}')},$$

where T is the volume of the crystal (the normalization constant is T^{-1}, and not $T^{-1/2}$, because f*f is integrated over both $\underline{r}$ and $\underline{r}'$). To determine the coefficients for this expansion, substitute the series into the differential equation for $g(\underline{r}-\underline{r}')$, take the derivatives of $f_{\underline{k}}$, multiply both sides by $f^*_{\underline{k}'}$, and then integrate over $\underline{r}$. The result is this expression for the expansion:

$$g(\underline{r},\underline{r}') = -\frac{1}{T}\sum_k \frac{e^{i\underline{k}\cdot(\underline{r}-\underline{r}')}}{\underline{k}^2-E}\,.$$

When this expression for $g(\underline{r},\underline{r}'+\underline{r}_s)$ is placed into Eq. 17,

$$G(\underline{r},\underline{r}') = \sum_s \{-\frac{1}{T}\sum_k \frac{e^{i\underline{k}\cdot(\underline{r}-\underline{r}'-\underline{r}_s)}}{\underline{k}^2-E}\}\, e^{i\underline{k}'\cdot\underline{r}_s}$$

$$= -\frac{1}{T}\sum_k \frac{e^{i\underline{k}\cdot(\underline{r}-\underline{r}')}}{\underline{k}^2-E}\{\sum_s e^{i(\underline{k}'-\underline{k})\cdot\underline{r}_s}\}\,.$$

The summation over s equals $N\delta(\underline{k}'-\underline{k}-\underline{K}_n)$. N is the number of unit cells in the crystal. The sum is zero unless $(\underline{k}'-\underline{k})$ is one of the translation vectors of the reciprocal lattice, $\underline{K}_n$. Summing over n to include every $\underline{k} = \underline{k}'+\underline{K}_n$ (and then dropping the now superfluous prime from $\underline{k}'$) gives the reciprocal lattice representation of the complete Green's function:

$$G(\underline{r},\underline{r}') = -\frac{1}{\tau}\sum_n \frac{e^{i(\underline{K}_n+\underline{k})\cdot(\underline{r}-\underline{r}')}}{(\underline{K}_n+\underline{k})^2-E} \qquad (22)$$

(note that $T = N\tau$, so that τ is, as before, the volume of a unit cell).

Inspection of the real or reciprocal lattice representation of $G(\underline{r},\underline{r}')$ reveals that the complete Green's function has these properties: G is a function of both $\underline{k}$ and E; it satisfies Bloch's theorem, $G(\underline{r}+\underline{r}_s,\underline{r}') = e^{i\underline{k}\cdot\underline{r}_s}G(\underline{r},\underline{r}')$; it is hermitian, $G(\underline{r},\underline{r}') = G^*(\underline{r}',\underline{r})$; it is singular when $\underline{r} = \underline{r}'$, due to the term in Eq. 21 in which $\underline{r}_s = \underline{r}_o = \underline{0}$; and due to the denominators in Eq. 22, G has singularities at those values of E equal to the free-electron energies, $(\underline{K}_n+\underline{k})^2$.

For crystals having more than one atom per unit cell, the complete Green's function may be represented in coordinates, $\underline{r}_j$ and $\underline{r}'_{j'}$, relative to a particular pair of atomic sites, j and j'. Choosing these coordinates for G is consistent with the commonplace and convenient use of functions centered on the atomic sites to represent the

potentials and wavefunctions present in a Schroedinger equation (Eq. 16) or a variational principle (Eq. 13). To change to these coordinates, simply let $\underline{r} = \underline{r}_j + \underline{a}_j$ and $\underline{r}' = \underline{r}'_{j'} + \underline{a}_{j'}$, where $\underline{a}_j$ and $\underline{a}_{j'}$ are the position vectors with respect to the origin of atomic sites j and j'. The real lattice representation of G then becomes

$$G^{(j,j')}(\underline{r}_j, \underline{r}'_{j'}) = -\frac{1}{4\pi} \sum_s e^{i\underline{k}\cdot\underline{r}_s} \frac{e^{i\kappa|\underline{r}_j - \underline{r}'_{j'} - \underline{r}_{sjj'}|}}{|\underline{r}_j - \underline{r}'_{j'} - \underline{r}_{sjj'}|}, \quad (23)$$

where $\underline{r}_{sjj'} = \underline{r}_s - \underline{a}_j + \underline{a}_{j'}$ is the vector from atomic site j in the central cell to atomic site j' in cell s. The reciprocal lattice representation of G becomes

$$G^{(j,j')}(\underline{r}_j, \underline{r}'_{j'}) = -\frac{1}{\tau} \sum_n \frac{e^{i(\underline{K}_n + \underline{k})\cdot(\underline{a}_j - \underline{a}_{j'})}}{(\underline{K}_n + \underline{k})^2 - E} \times e^{i(\underline{K}_n + \underline{k})\cdot(\underline{r}_j - \underline{r}'_{j'})}. \quad (24)$$

In Eq. 22 or Eq. 24, the complete Green's function is expanded in functions that describe the motion of a free particle having a definite linear momentum. G can also be expanded in functions that describe the motion of a free particle having a definite angular momentum:

$$G^{(j,j')}(\underline{r}, \underline{r}'_{j'}) = \sum_{\ell m} \sum_{\ell' m'} \Big[A^{(j,j')}_{\ell m, \ell' m'} j_\ell(\kappa r_j) j_{\ell'}(\kappa r'_{j'}) + \kappa \delta_{jj'} \delta_{\ell\ell'} \delta_{mm'} j_\ell(\kappa r_j) n_{\ell'}(\kappa r'_{j'}) \Big] Y_{\ell m}(\hat{r}_j) Y^*_{\ell' m'}(\hat{r}'_{j'}). \quad (25)$$

$A^{(j,j')}_{\ell m, \ell' m'}$ is an expansion coefficient, j_ℓ is a spherical Bessel function, and n_ℓ is a spherical Neumann function. Making this

expansion of G is a complicated analytical problem, and care must be taken to deal correctly with the singularity of G when $\underline{r} = \underline{r}'$. The form of G in Eq. 25 holds for $r_j < r'_{j'}$, when $j = j'$, and for $(r_j + r'_{j'}) < |\underline{a}_j - \underline{a}_{j'}|$ when $j \neq j'$.

The KKR secular equation in its standard form

To arrive at last at the secular equation of the KKR method, substitute Eq. 20 for the trial wavefunction $\psi^{j'}$ and Eq. 25 for the complete Green's function $G^{(j,j')}$ into the surface condition they should satisfy, Eq. 19, multiply by $Y^*_{L'M'}(\hat{r}_j)$ and integrate out all angular dependence from the equation:

$$\sum_{j'LM} \sum_{\ell m} \sum_{\ell'm'} \left[R_L^{j'} \frac{d}{dr'_{j'}} G^{(j,j')}_{\ell m,\ell'm'} - G^{(j,j')}_{\ell m,\ell'm'} \frac{d}{dr'_{j'}} R_L^{j'} \right] c_{LM}^{j'} \times \int d\Omega_j Y_{\ell m}(\hat{r}_j) Y^*_{L'M'}(\hat{r}_j) \int ds' Y_{LM}(\hat{r}'_{j'}) Y^*_{\ell'm'}(\hat{r}'_{j'}) = 0. \tag{26}$$

The dependence of $R_L^{j'}$ on E and $r'_{j'}$, and of $G^{(j,j')}_{\ell m,\ell'm'}$ on r_j and $r'_{j'}$, is understood in Eq. 26. $G^{(j,j')}_{\ell m,\ell'm'}$ is the bracketted term in Eq. 25. Because G is singular when $\underline{r} = \underline{r}'$, a limiting procedure must be used to evaluate integrals involving G taken over $\underline{r}$ or $\underline{r}'$. This is done by evaluating the surface integrals in Eq. 19 over spheres of radius $r'_{j'} = R_{j'} - \varepsilon$. When j and j' are the same, $\underline{r}$ is restricted to the sphere $r_j = R_j - 2\varepsilon$, so that $\underline{r}_j$ never equals $\underline{r}'_{j'}$. After all else is done, the limit $\varepsilon \to 0$ is taken.

The integral over the surface area s' equals $R^2_{j'}\delta_{L\ell'}\delta_{Mm'}$, and the integral over the solid angle Ω_j equals $\delta_{L'\ell}\delta_{M'm}$. Eq. 26 then becomes

$$\sum_{j'\ell'm'}\left[R^{j'}_{\ell'}\frac{d}{dr'_{j'}}G^{(j,j')}_{\ell m,\ell'm'} - G^{(j,j')}_{\ell m,\ell'm'}\frac{d}{dr'_{j'}}R^{j'}_{\ell'}\right] \times R^2_{j'}c^{j'}_{\ell'm'} = 0 . \qquad (27)$$

Note that in Eqs. 26 and 27 the arguments of R and G are going to have the values $r_j = R_j - 2\varepsilon$ and $r'_{j'} = R_{j'} - \varepsilon$. Substituting the bracketted term in Eq. 25 for G, taking the derivatives of R and G with respect to $r'_{j'}$, dividing through by $j_\ell(Kr_j)$ to leave functions only of $r'_{j'}$, and rearranging terms gives

$$\sum_{j'\ell'm'}\left[A^{(j,j')}_{\ell m,\ell'm'} + \delta_{jj'}\delta_{\ell\ell'}\delta_{mm'}\,\kappa\,\frac{Rn'-R'n}{Rj'-R'j}\right]\bar{c}^{j'}_{\ell'm'} = 0, \qquad (28)$$

where $\bar{c}^{j'}_{\ell'm'} = R^2_{j'}(Rj'-R'j)c^{j'}_{\ell'm'}$. (29)

Once the limit $\varepsilon\to 0$ has been taken,

$$R = R^{j'}_{\ell'}(R_{j'}),\quad R' = \frac{d}{dr'_{j'}}R^{j'}_{\ell'}(r'_{j'})\Big|_{r'_{j'}=R_{j'}},$$

$$j = j_{\ell'}(\kappa R_{j'}),\quad j' = \frac{d}{dr'_{j'}}j_{\ell'}(\kappa r'_{j'})\Big|_{r'_{j'}=R_{j'}},$$

$$n = n_{\ell'}(\kappa R_{j'}),\quad n' = \frac{d}{dr'_{j'}}n_{\ell'}(\kappa r'_{j'})\Big|_{r'_{j'}=R_{j'}}.$$

Eq. 28 defines a system of linear equations which have non-trivial solutions when the determinant of their coefficients equals zero:

$$\text{Det} \left| A^{(j,j')}_{\ell m,\ell' m'} + \delta_{jj'}\delta_{\ell\ell'}\delta_{mm'} \kappa \frac{n'-nL}{j'-jL} \right| = 0 \ , \qquad (30)$$

where $L = R'/R$ is the logarithmic derivative of the energy-dependent radial function $R^{j'}_{\ell',E}$ at the MT radius $R_{j'}$.
Eq. 30 is the KKR secular equation. It determines the relationship between E and $\underline{k}$ that is needed to calculate the energy bands of a perfect crystal.

CHAPTER IV. THE CALCULATIONS AND THEIR COMPARISON WITH SOME EXPERIMENTS

If sodium tungsten bronze were stoichiometric $NaWO_3$, its crystals would have the perovskite structure depicted in Figure 1. The Bravais lattice is simple cubic, and the space group is O_h^1. Using the primitive lattice translation vectors as the basis, the positions of the atoms in the unit cell may be indicated by choosing the coordinates (0,0,0) for W, (1/2,0,0) for O_1, (0,1/2,0) for O_2, (0,0,1/2) for O_3, and (1/2,1/2,1/2) for Na. The point symmetry at both the W and Na sites is O_h, and that at the O sites is D_{4h}. The lattice constant was taken to be 3.860 Å (35). Values calculated for the bond lengths are 1.930 Å for W-O, 3.343 Å for W-Na, and 2.729 Å for O-Na.

The muffin-tin radii were determined by the following considerations. The MT radius of Na is limited only by the dimensions of the unit cell. The sum of the W and O MT radii equals the lattice constant, but their ratio may vary between the points where one or the other of their spheres touches the Na sphere. This leaves considerable freedom of choice for the W and O radii, at least ±0.3 Å. In the absence of any geometrical ground for fixing the radii, the decision taken was to use the Bragg-Slater atomic radii, 1.35 Å for W, 0.60 Å for O, and 1.80 Å for Na (88), as a criterion. These radii are quite successful in reproducing observed interatomic

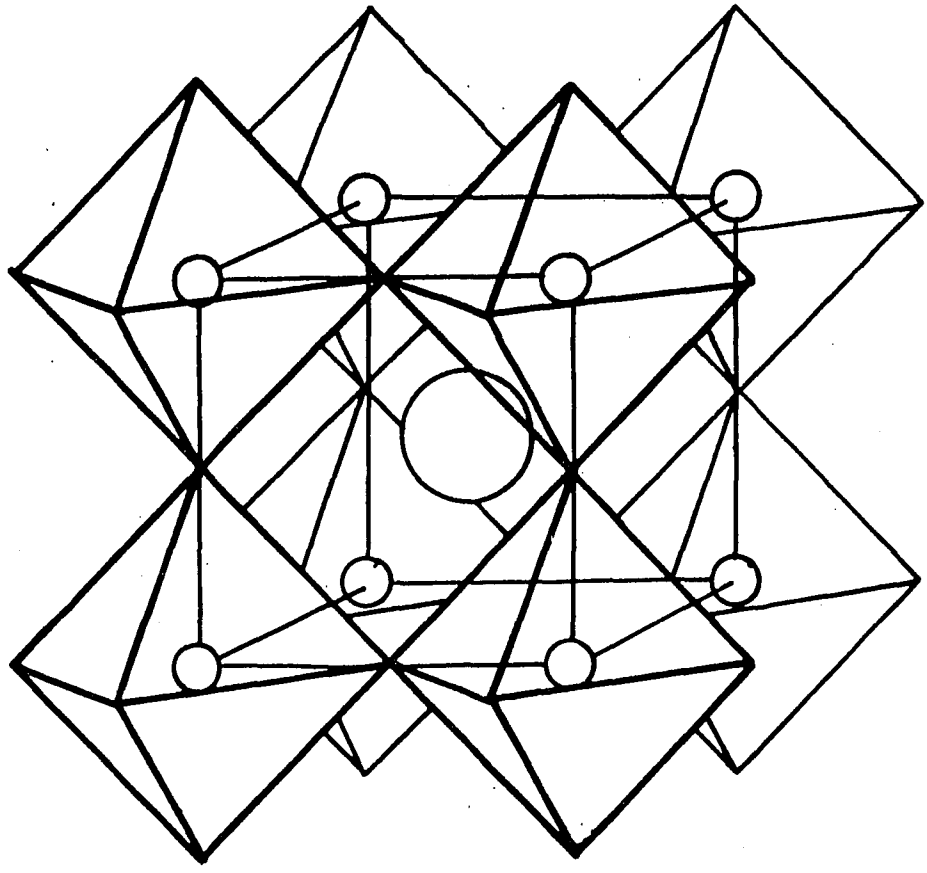

Figure 1. Crystal structure of cubic $NaWO_3$. A sodium atom lies at the center of a cubic cell, a tungsten atom is at each corner, and an oxygen atom is at the midpoint of each edge

distances, and they correlate well with computed radii of the maximum radial charge density in the outermost shells of the atoms. Note that these radii nearly give the calculated W-O bond length. The actual MT radii used were those points on the logarithmic radial (Weber) mesh closest to the Bragg-Slater radii: 1.310 Å for W, 0.600 Å for O, and 1.848 Å for Na. With this choice, over 67% of the unit cell volume lies within the MT spheres. The relative sizes of these MT spheres are illustrated in Figure 2.

The atomic configuration of W is $(Xe)4f^{14}5d^{4}6s^{2}$, of O is $(He)2s^{2}2p^{4}$, and of Na is $(Ne)3s^{1}$. The crystalline potentials were constructed from the Hartree-Fock-Slater atomic charge densities for these configurations (89) by using the ad hoc method of Mattheiss (90). Full Slater exchange was assumed (75). To guarantee a valid comparison between them, the WO_3, $\square WO_3$, and $NaWO_3$ band calculations were kept the same in all ways but one; in construction of the crystalline potentials, where contributions from neutral sodium atoms either were not (WO_3 and $\square WO_3$) or were ($NaWO_3$) included. In the $\square WO_3$ calculation a muffin-tin sphere was centered on the sodium vacancy $\square$ (91,92). This sphere serves to take into account the significant variation of the interstitial potential that is characteristic of open crystal structures. Moreover, by treating the $\square$ and Na identically, this artifice provides a bona fide basis for analysis of the

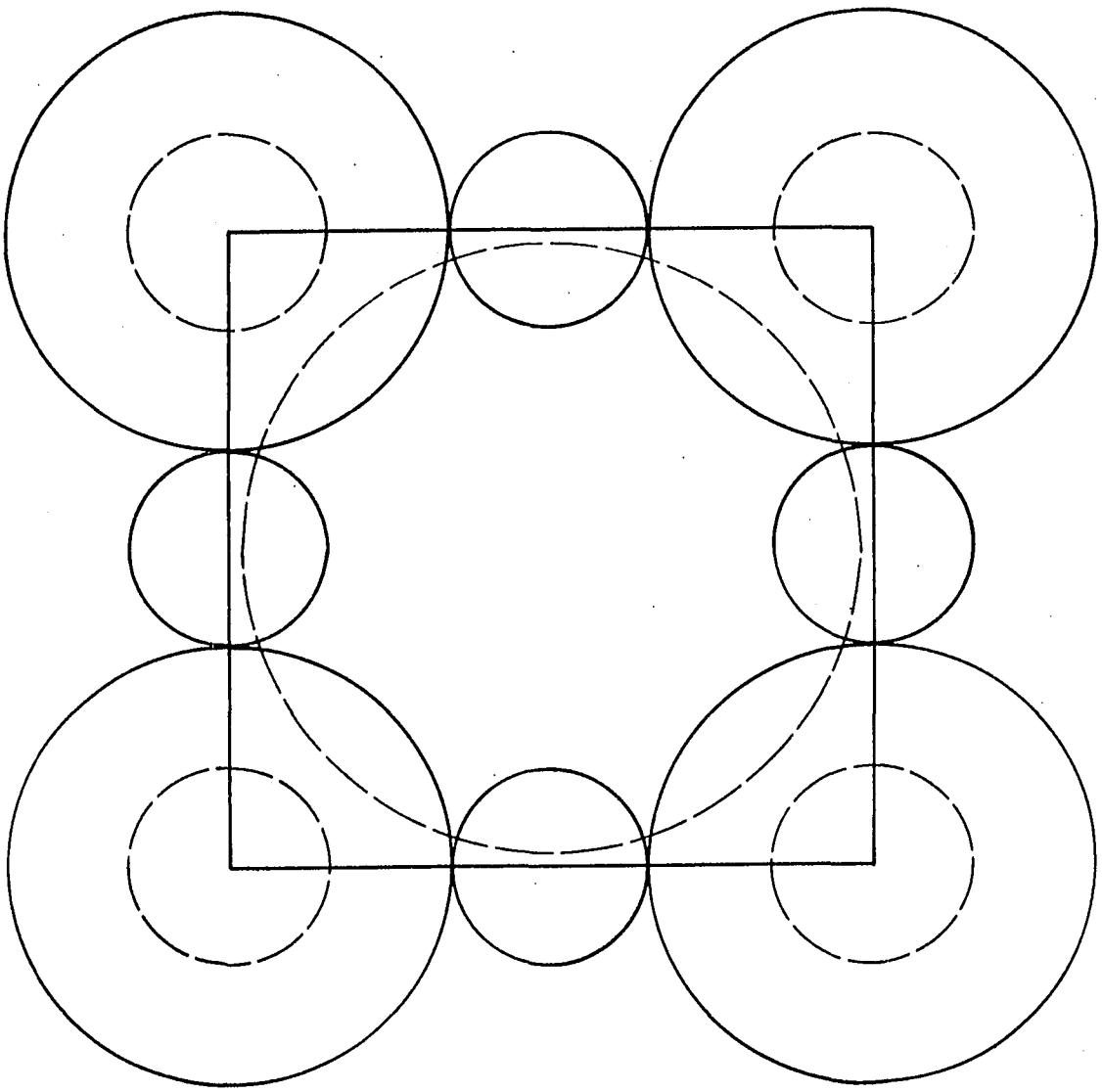

Figure 2. Muffin-tin spheres about each atomic site in $NaWO_3$ projected onto the basal plane. The radii shown closely approximate those used in the calculations. Solid circles are for spheres about sites that lie in the basal plane; dashed circles are for those that are a distance a/2 above the basal plane

sodium atom's influence on the crystalline potential and, consequently, on the band structure. The average potential in the interstitial region, the reference point taken for the muffin-tin potential, was -1.171 Ry for WO_3, -1.614 Ry for $\square WO_3$, and -1.730 Ry for $NaWO_3$.

A nonself-consistent and nonrelativistic version of the KKR method was used to perform the calculations. Details obtained at this level of approximation may, of course, change when the model is improved; so care must be taken to base interpretations upon those features expected to be unaffected by improvements. Nonetheless, there is cause for confidence in nonself-consistent results when using full Slater exchange. Snow and Waber (93), Connolly (94), Papaconstantopoulos et al. (95), and Anderson et al. (96) found from their respective self-consistent calculations on Cu, Ni, V, and Nb that the interplay of configuration and exchange led to astonishing over-all agreement between non-self-consistent results using full Slater (α=1) exchange and self-consistent results using less than full Slater exchange. Recent calculations by Walch and Ellis (97) on MgO, Myron and Freeman (98) on TiS_2, and Moruzzi et al. (99) on β-brass (CuZn), support the same conclusion for compounds, even when there is evidence of charge transfer. Perhaps of more concern is the spherical averaging of the potentials inside the muffin-tin spheres. This averaging acts counter

to any tendency towards the directional bonding one might expect in these compounds, particularly between the W and O atoms.

The band calculations used s, p, and d radial functions in each muffin-tin sphere. Therefore, the order of the KKR matrix was 36 for WO_3 and 45 for $\square WO_3$ and $NaWO_3$. The matrix elements were evaluated by using the method developed by Ham and Segall (81-83). The real and reciprocal lattice sums were truncated to 33 and 96 terms, respectively, and the Ewald parameter which produced convergence was found to be 0.3. The accuracy to which each matrix element was calculated was 10^{-5} Ry^{-1}.

The Brillouin zone for a simple cubic Bravais lattice is shown in Figure 3, with the high symmetry points and lines that bound an irreducible 1/48th of the zone labeled as has become standard. Energy eigenvalues were calculated on a uniform, 56 point, $\pi/5a$ mesh in this irreducible part of the zone (Figure 4). These points, ordered as they were when the calculations were performed, with their degeneracy and their coordinates, are listed in Table 1. Over an energy range 1.2 Ry wide, up to 16 eigenvalues were found at a $\underline{k}$-point. An iterative procedure was used to find each eigenvalue to within ±0.001 Ry.

The results of these calculations, shown in Figures 5, 6, and 7, clearly demonstrate how small an influence Na has

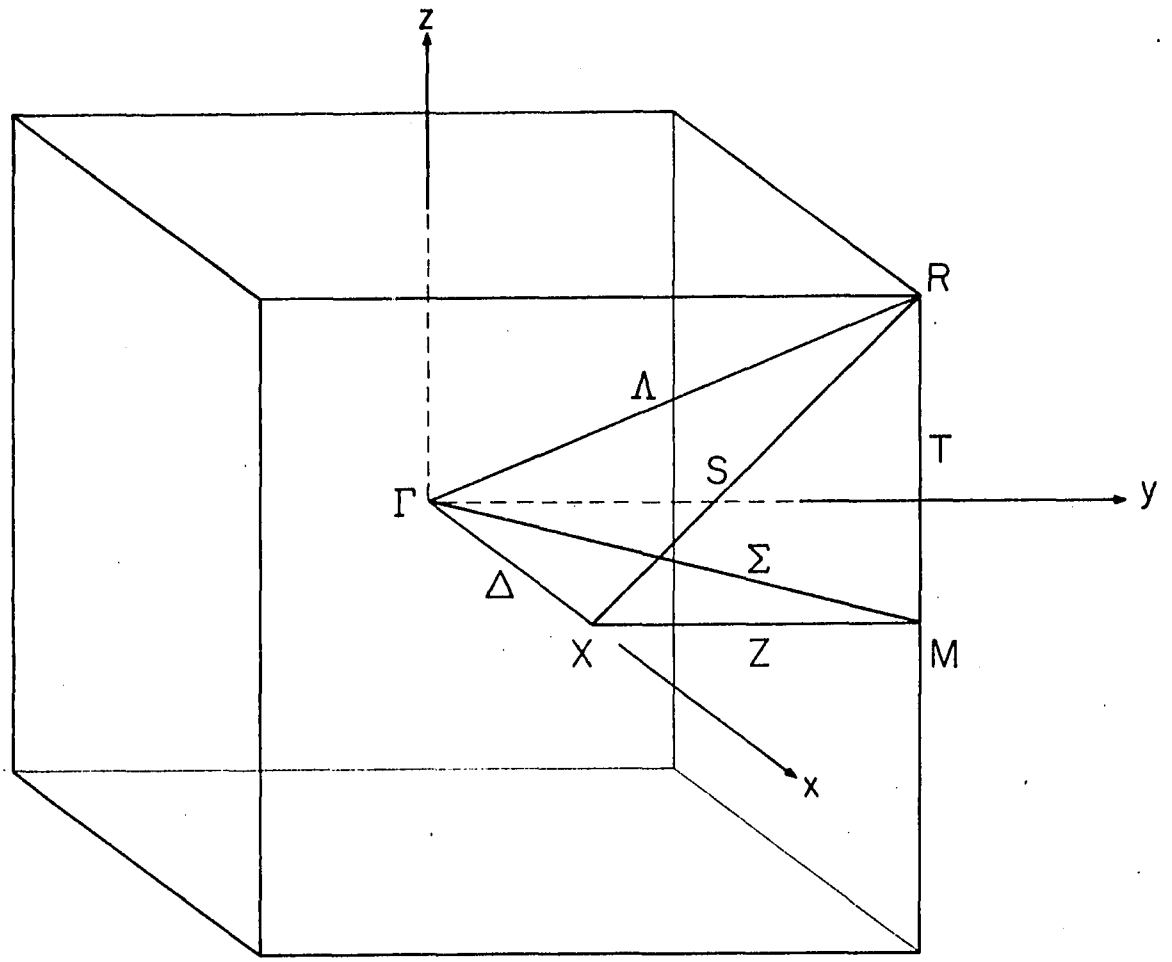

Figure 3. Brillouin zone for a simple cubic Bravais lattice. An irreducible 1/48th part of the full zone is shown with the designations due to Bouckaert, Smoluchowski, and Wigner for the high symmetry points and lines

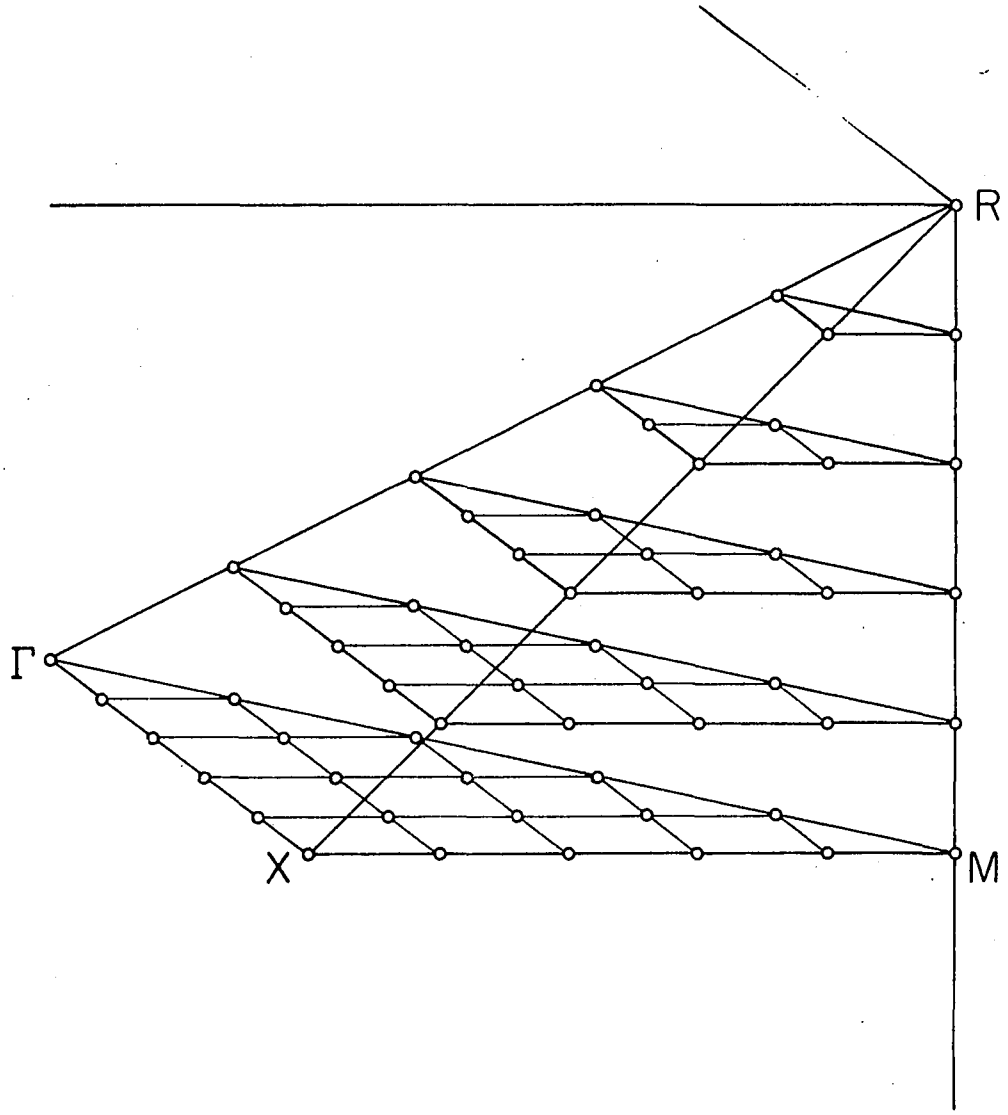

Figure 4. Points of a π/5a mesh in an irreducible wedge of the Brillouin zone at which a full KKR calculation was performed

Table 1. The 56 $\underline{k}$-points at which a full KKR calculation was performed: their index i, degeneracy g, and coordinates in units of 0.2 π/a

i	g	5 a/π (k_x,k_y,k_z)	i	g	5 a/π (k_x,k_y,k_z)	i	g	5 a/π (k_x,k_y,k_z)
1	1	(0,0,0)	20	12	(5,1,0)	39	24	(4,4,2)
2	12	(1,1,0)	21	3	(5,0,0)	40	6	(5,5,2)
3	12	(2,2,0)	22	8	(1,1,1)	41	24	(3,2,2)
4	12	(3,3,0)	23	24	(2,2,1)	42	48	(4,3,2)
5	12	(4,4,0)	24	24	(3,3,1)	43	24	(5,4,2)
6	3	(5,5,0)	25	24	(4,4,1)	44	24	(4,2,2)
7	6	(1,0,0)	26	6	(5,5,1)	45	24	(5,3,2)
8	24	(2,1,0)	27	24	(2,1,1)	46	12	(5,2,2)
9	24	(3,2,0)	28	48	(3,2,1)	47	8	(3,3,3)
10	24	(4,3,0)	29	48	(4,3,1)	48	24	(4,4,3)
11	12	(5,4,0)	30	24	(5,4,1)	49	6	(5,5,3)
12	6	(2,0,0)	31	24	(3,1,1)	50	24	(4,3,3)
13	24	(3,1,0)	32	48	(4,2,1)	51	24	(5,4,3)
14	24	(4,2,0)	33	24	(5,3,1)	52	12	(5,3,3)
15	12	(5,3,0)	34	24	(4,1,1)	53	8	(4,4,4)
16	6	(3,0,0)	35	24	(5,2,1)	54	6	(5,5,4)
17	24	(4,1,0)	36	12	(5,1,1)	55	12	(5,4,4)
18	12	(5,2,0)	37	8	(2,2,2)	56	1	(5,5,5)
19	6	(4,0,0)	38	24	(3,3,2)			

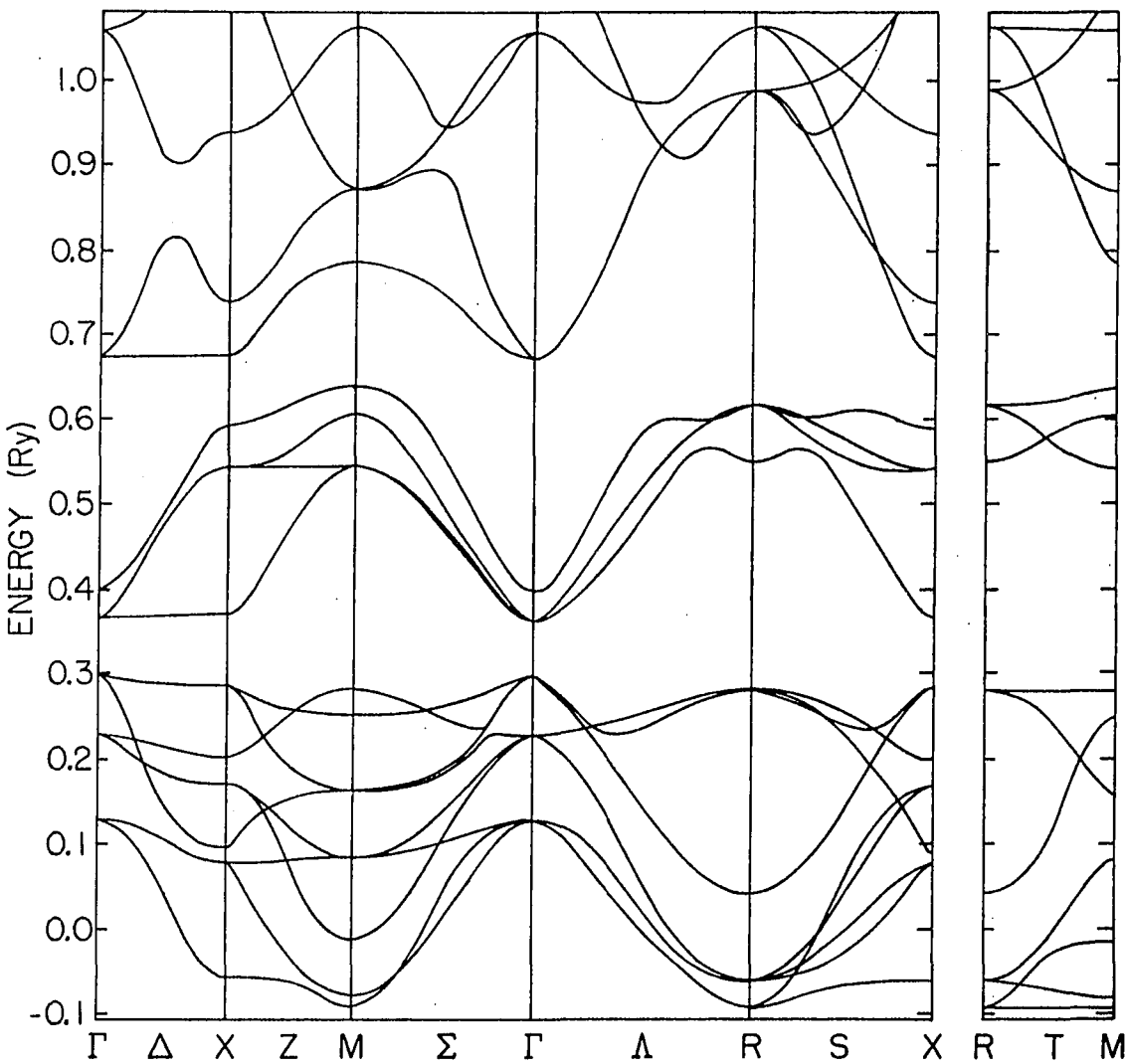

Figure 5. Energy bands of WO_3 along the symmetry axes

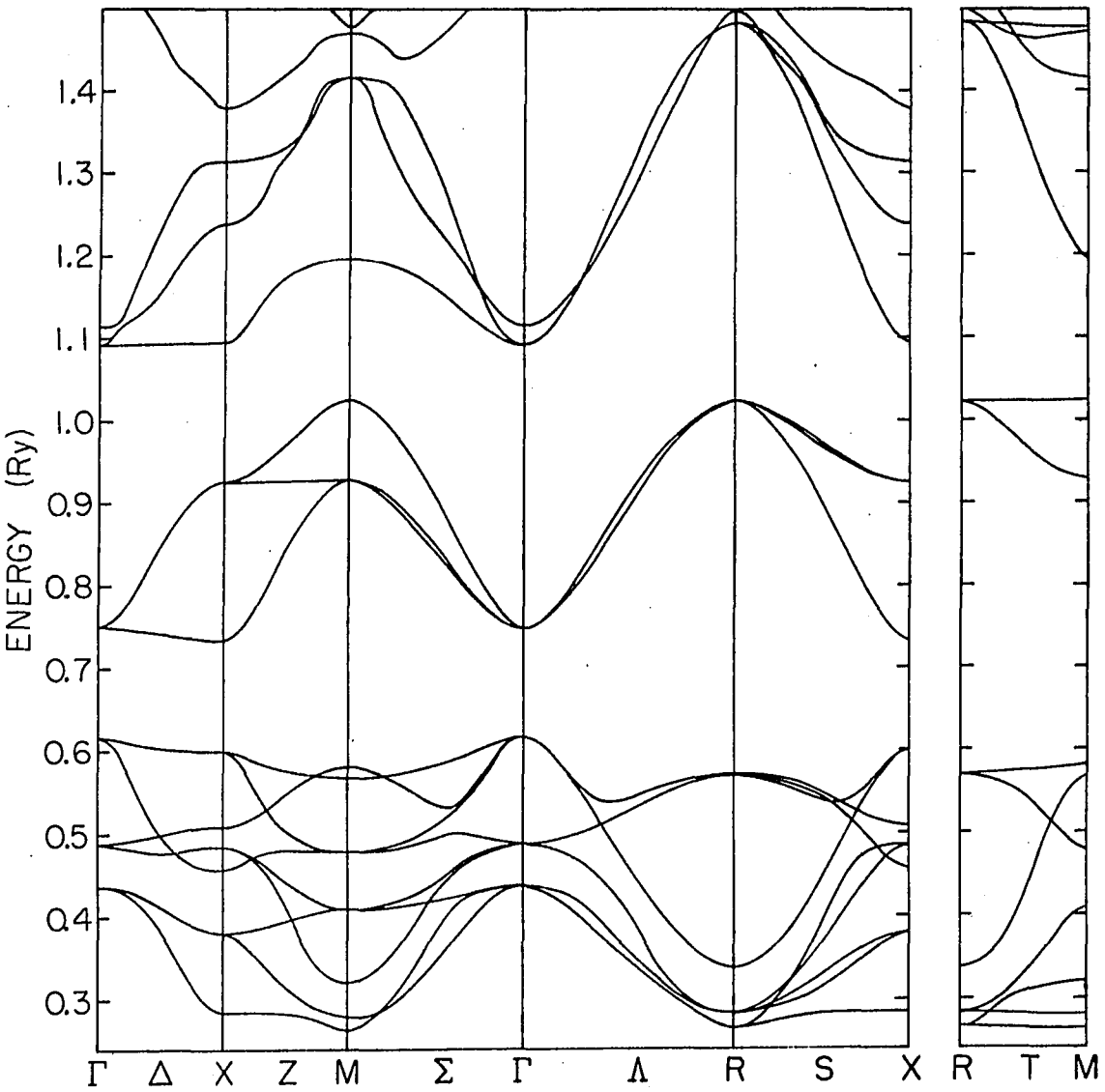

Figure 6. Energy bands of □WO_3 along the symmetry axes

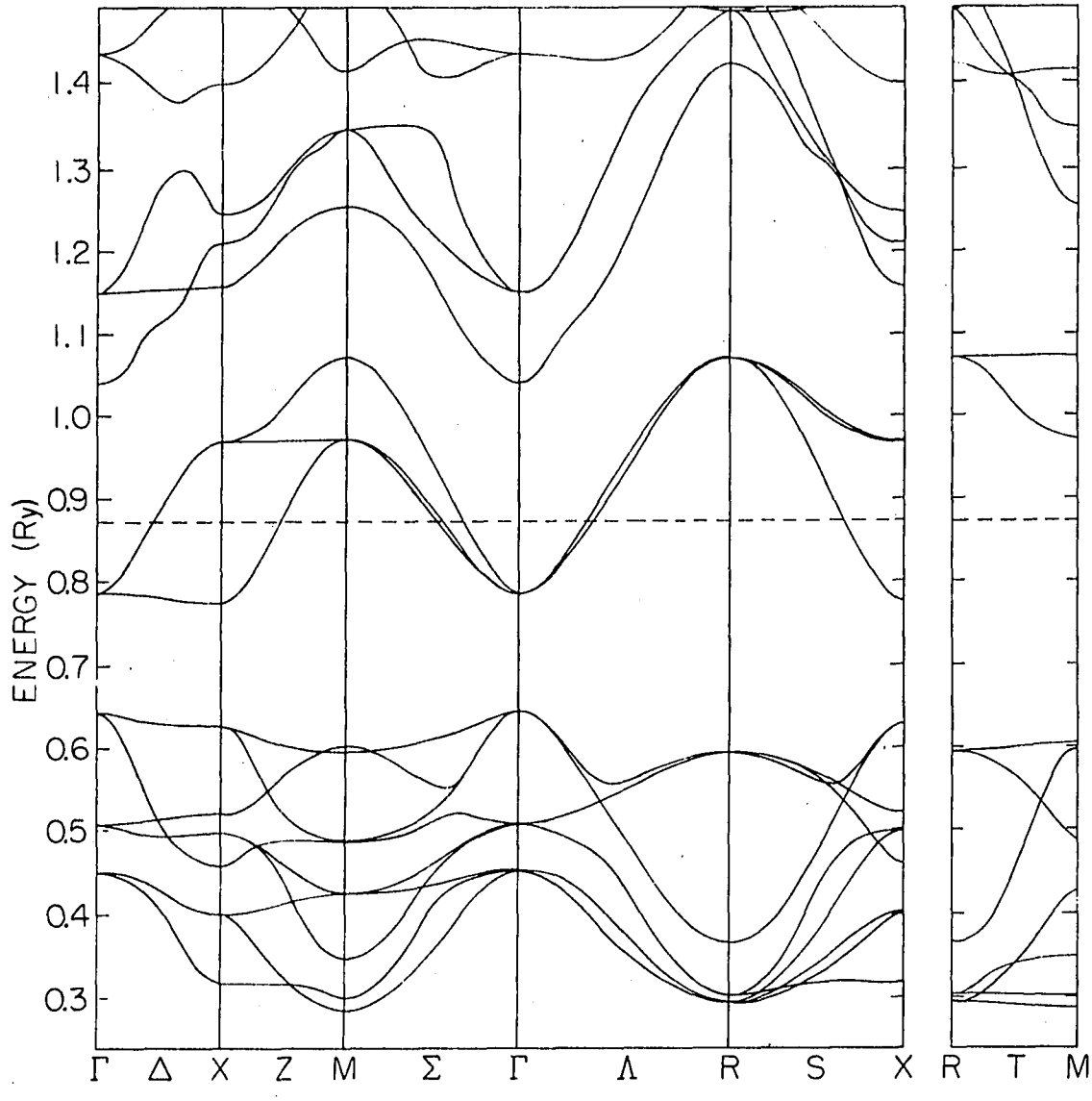

Figure 7. Energy bands of $NaWO_3$ along the symmetry axes. The dashed line marks the Fermi energy (0.876 Ry)

on the structure of the valence and lowest conduction bands. The largest modification of the $\square WO_3$ band structure occurs among the higher energy states, where the presence of Na shifts the 15th band (numbering the bands in ascending order of energy) downward (this band corresponds to the band arising from Γ_1 in Mattheiss' ReO_3 (8) calculation). The complex structure of these higher states comes from the crossing and strong mixing of this band with the 13th and 14th (e_g or Γ_{12}) bands (for comparison, Mattheiss' ReO_3 calculation places the Γ_1 band completely above the Γ_{12} bands). There are slight shifts of some of the valence bands toward lower energy. There is also a slight rise of the conduction bands relative to the valence bands caused by their increased occupation giving rise to an increased coulomb repulsion for these states. Since the shape of the conduction bands remains essentially constant, the rigid band model will be valid for electronic properties depending on only these states.

Why the $\square WO_3$ electronic structure changes so little when Na is introduced may be understood simply by considering the $\square$ and Na muffin-tin potentials. The $\square$ potential is a hill-shaped barrier arising from the coulomb and (Slater) exchange contributions made by the W and O atoms surrounding the interstitial region. Adding in the potential contributions from neutral Na atoms affects the crystalline potential

in two main ways. It significantly lowers the muffin-tin zero, and it lowers the potential barrier about the Na site, leaving a hill that rings the Na potential well. Since the Na muffin-tin potential, over a sizable volume, is repulsive with respect to the average interstitial potential, thinking of the Na as a Na ion may be an oversimplification. What is remarkable about the □ and Na muffin-tin potentials is that the □ potential in $\square WO_3$ effectively acts as a pseudopotential for the Na in $NaWO_3$. The □ potential barrier appears merely to mimic the cancellation of the core potential typical of pseudopotentials. The Na sublattice seemingly contributes a nearly flat potential, analogous to that of Na metal, changing the energy zero with hardly any change in energy band structure. In fact, the shortest Na-Na distance in $NaWO_3$ is only a little longer than the nearest-neighbor Na-Na distance in Na metal. Radial distribution functions calculated using the □ and Na muffin-tin potentials are very similar throughout the energy range of the valence and lowest conduction bands. Their most significant difference is the absence of radial nodes in the □ functions, since there are no bound states to which they must be orthogonal (this is typical of pseudowavefunctions). Their likeness, together with the likeness of the W and O radial functions in $\square WO_3$ and $NaWO_3$, implies similar sets of logarithmic derivatives, and therefore similar electronic structures.

For the calculation of the density of states and the Fermi surface, a least-squares Fourier fit was made to the energy bands at the calculated $\underline{k}$-points. This fitting was done with the first 30 symmetrized plane waves in reciprocal space:

$$E_n(\underline{k}) = \sum_{\ell} c_{n\ell} S_{\ell}(\underline{k}),$$

where $S_{\ell}(\underline{k}) = \frac{1}{g} \sum_{\alpha=1}^{g} e^{i\underline{k}\cdot\alpha\underline{R}_{\ell}}$.

The number of operations α in the point group of the crystal is g (48 for cubic symmetry). $\underline{R}_{\ell}$ is a translation vector in the real lattice. The Fourier coefficients, $c_{n\ell}$, were used to evaluate energies at arbitrary points in the Brillouin zone. This type of fit cannot represent energies near band crossings accurately, and spurious structure in the density of states or Fermi surface may result from this defect. The maximum errors and root-mean-square errors of this fit to the first 12 bands calculated are listed in Table 2.

Density of states histograms were calculated using the linear analytic tetrahedron method (100,101). The irreducible 1/48th of the Brillouin zone, itself an irregular tetrahedron, was subdivided into a large number of small tetrahedra. Within each tetrahedral microzone a surface of constant energy was approximated by a plane. This linear interpolation is determined uniquely by the

Table 2. Maximum error, Δ_{max}, and root-mean-square error, Δ_{rms}, of the Fourier fit to the 56 $\underline{k}$-points calculated for the valence and lowest conduction bands of WO_3, $\square WO_3$, and $NaWO_3$

	WO_3		$\square WO_3$		$NaWO_3$	
Band	Δ_{max}	Δ_{rms}	Δ_{max}	Δ_{rms}	Δ_{max}	Δ_{rms}
1	5.7	2.9	6.0	3.2	2.9	1.1
2	3.7	1.7	3.9	1.9	6.5	2.8
3	8.3	3.3	7.2	3.4	6.7	3.5
4	6.9	3.3	6.1	2.3	6.4	2.8
5	5.5	2.3	12.3	5.0	15.5	5.0
6	13.4	6.8	14.5	7.0	15.7	8.3
7	8.6	2.7	7.0	3.1	9.1	4.0
8	14.4	6.4	17.5	7.8	19.0	8.1
9	11.7	4.9	10.8	5.3	11.4	5.7
10	6.7	2.0	7.0	2.4	7.2	2.5
11	5.4	1.8	8.1	3.6	6.9	3.1
12	4.6	1.3	4.8	1.9	5.9	2.0

energy values at the four corners of a tetrahedron, and leads to analytic expressions for the surface area and the occupied volume inside each one. The four corner energies were calculated with the Fourier fit coefficients. These energies and the volume of the tetrahedron determine the contribution to the density of states from one microzone. Among the advantages of this method are that the shape of the tetrahedron is irrelevant, that the interpolation is continuous throughout the Brillouin zone, and that energy gradients do not occur explicitly. The convergence of this method as the Brillouin zone is further divided is shown in Figure 8. The density of states for the valence and lowest conduction band of $NaWO_3$ is shown in Figure 9, and the densities of states from all three band calculations are compared in Figure 10, together with their integrated densities of states.

The dominant features of the conduction band density of states can be obtained from a simple LCAO model in which the conduction band width is due entirely to W-O pdπ interaction. Wolfram (102) has noted that in this model the energy bands have a two-dimensional character, that $E(\underline{k})$ depends upon only two components of the wave vector, and that this requires the density of states to have a logarithmic singularity in the interior of the band and discontinuities at the band edges.

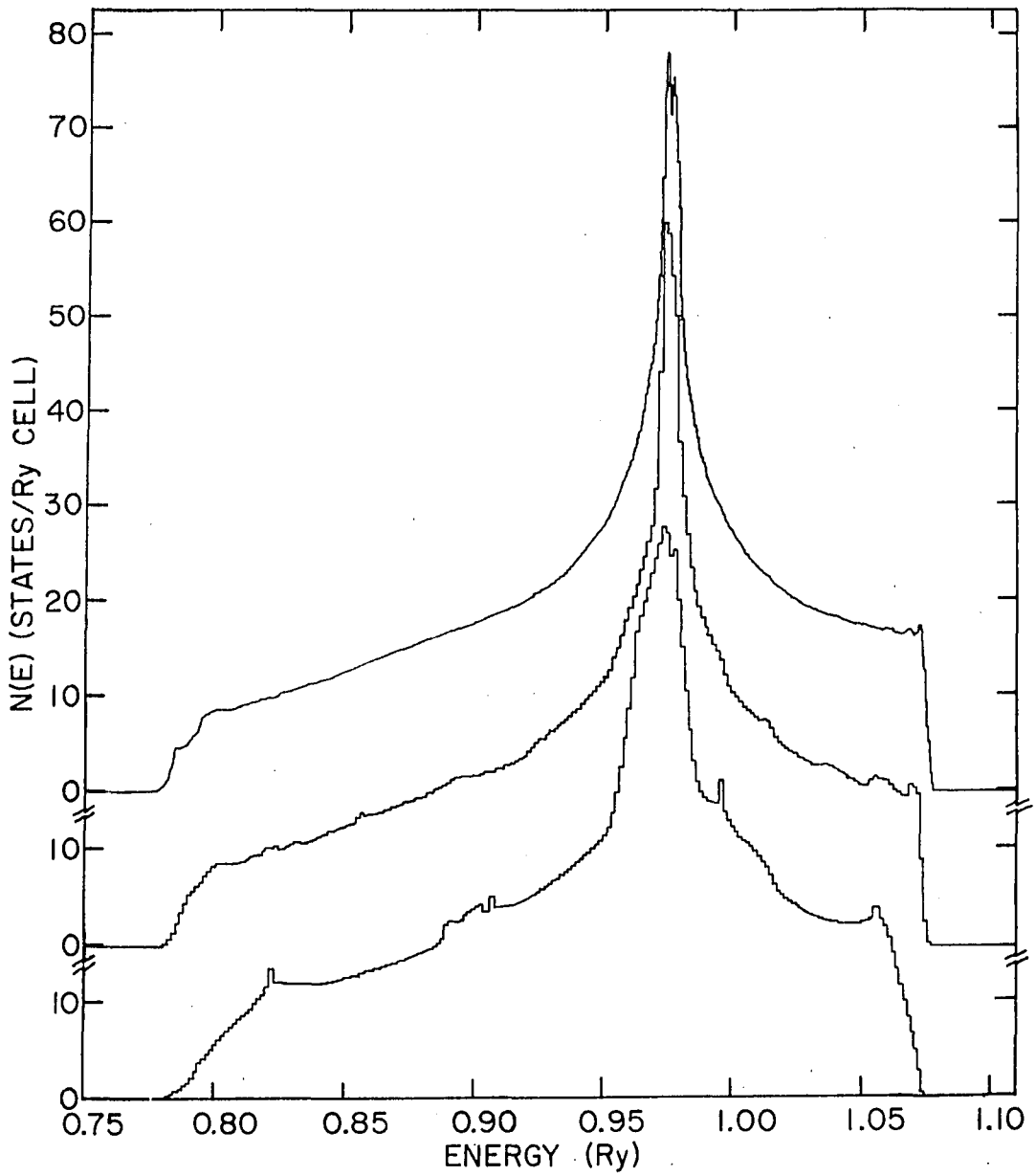

Figure 8. Convergence of the density of states calculated using the linear analytic tetrahedron method. The density of states of the conduction band of $NaWO_3$ is shown for subdivision of an irreducible zone into 512 (bottom), 4096 (middle), and 32768 (top) tetrahedra

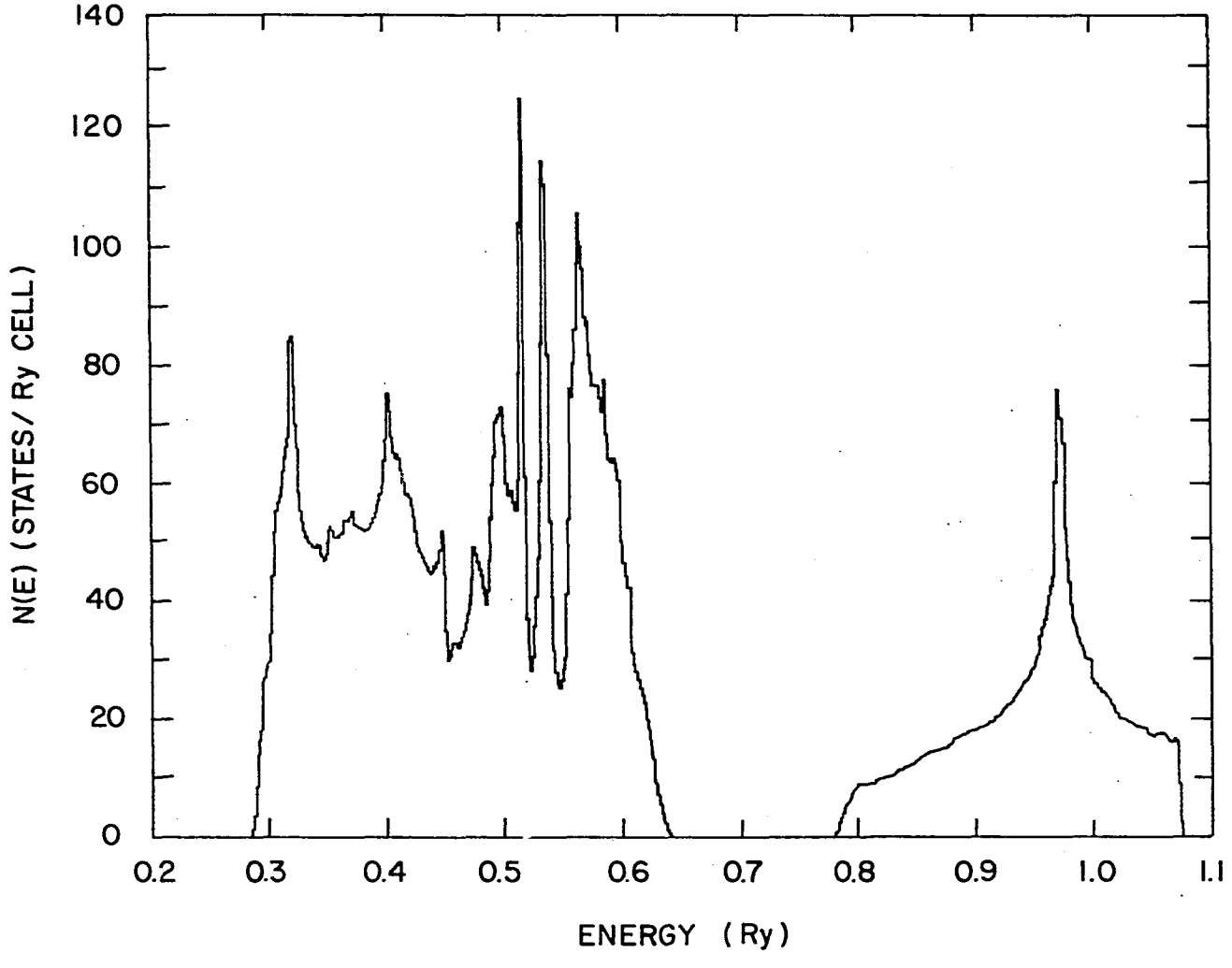

Figure 9. Density of states of $NaWO_3$

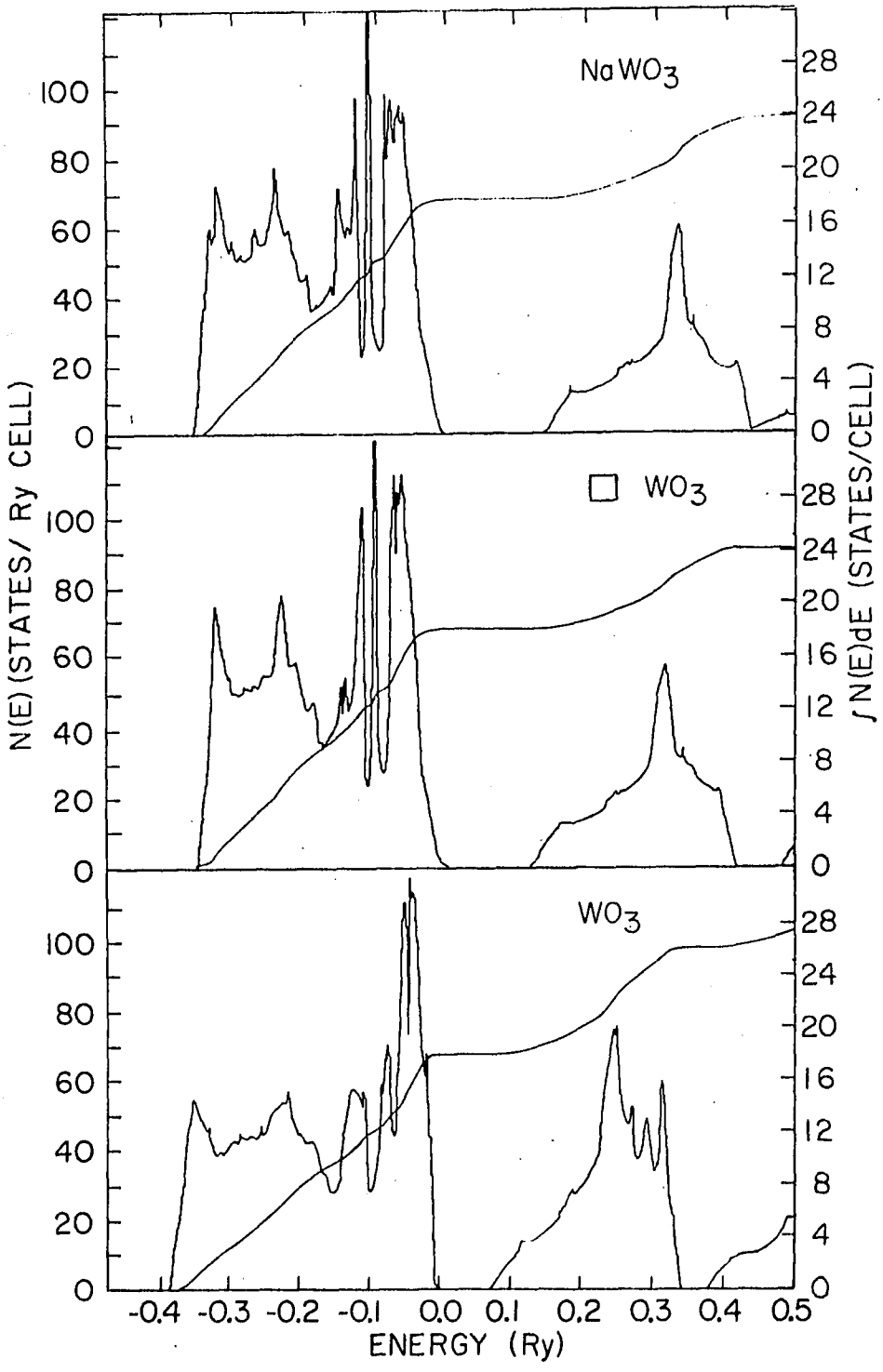

Figure 10. Comparison of the densities of states and integrated densities of states of WO_3, $\square WO_3$, and $NaWO_3$

The results of the calculation of the $NaWO_3$ Fermi surface are presented in Figures 11, 12, and 13. The three bands that cross the Fermi energy create the three sheets of the Fermi surface, labeled by Mattheiss (8) α, β, and γ. These sheets are electron-like surfaces centered about Γ. α and β are closed, and γ is open along [100]. All three are pieces from three cylinders extended along the [100] directions. These pieces separate where the cylinders intersect. This is clearly seen in the cross section of the Fermi surface in the (100) plane (Figure 12). The diameter of the cylinders is quite uniform. Much of the curvature evident in Figure 12 comes from the Fourier fit to the energy bands.

Campagna et al. (103) measured the X-ray photoemission spectrum of Na_xWO_3 for the nominal compositions $x = 0.620$, 0.764, and 0.805. Their data seem to substantiate the similarity of the Na_xWO_3 and ReO_3 electronic structures. They found an increase in the area of the conduction band peak near the Fermi energy proportional to the sodium concentration. This result provides direct evidence for the participation of the sodium valence electron in the filling of the conduction band. In Figures 14, 15, and 16 their data are compared with the calculated density of states below the Fermi level. This comparison indicates that the conduction band below the Fermi energy is 12.5 ± 7.5

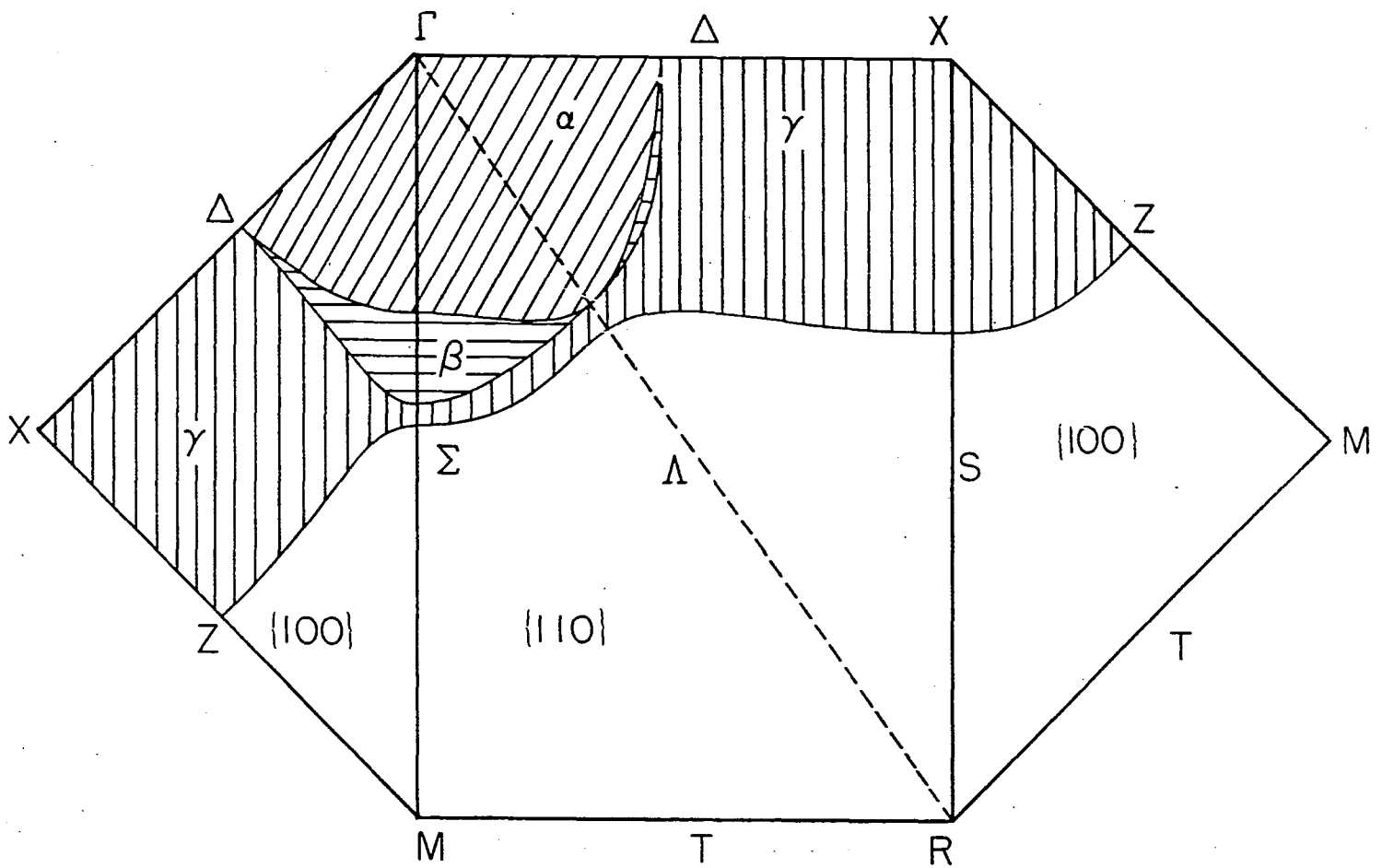

Figure 11. Sheets of the $NaWO_3$ Fermi surface, α, β, and γ, for the three bands that cross the Fermi level. The surface is represented by its intersection with the planes that bound an irreducible zone

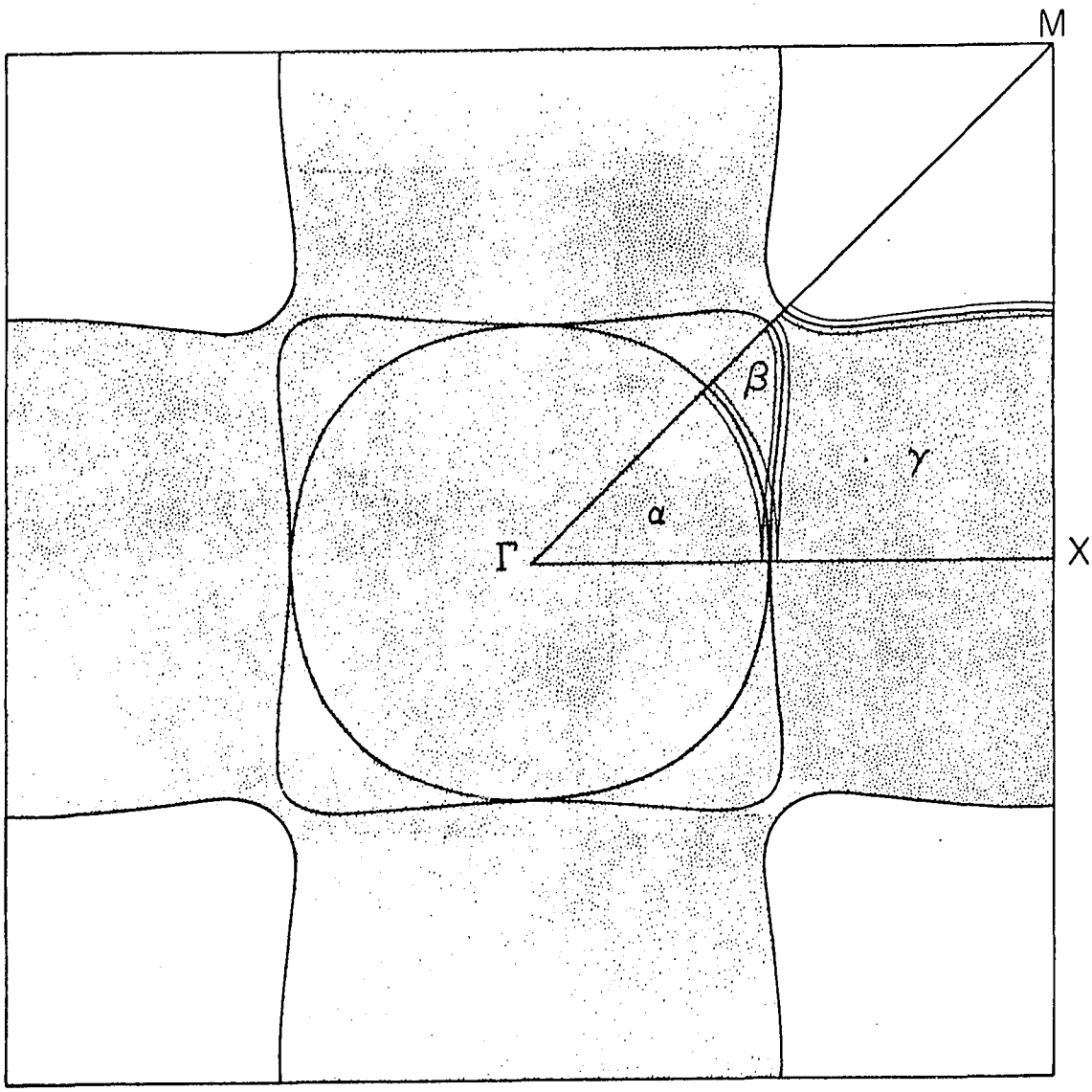

Figure 12. Cross section of the $NaWO_3$ Fermi surface in the (100) plane. The additional lines in the ΓXM section indicate the change in the Fermi surface due to a shift in the Fermi energy of ±0.002 Ry

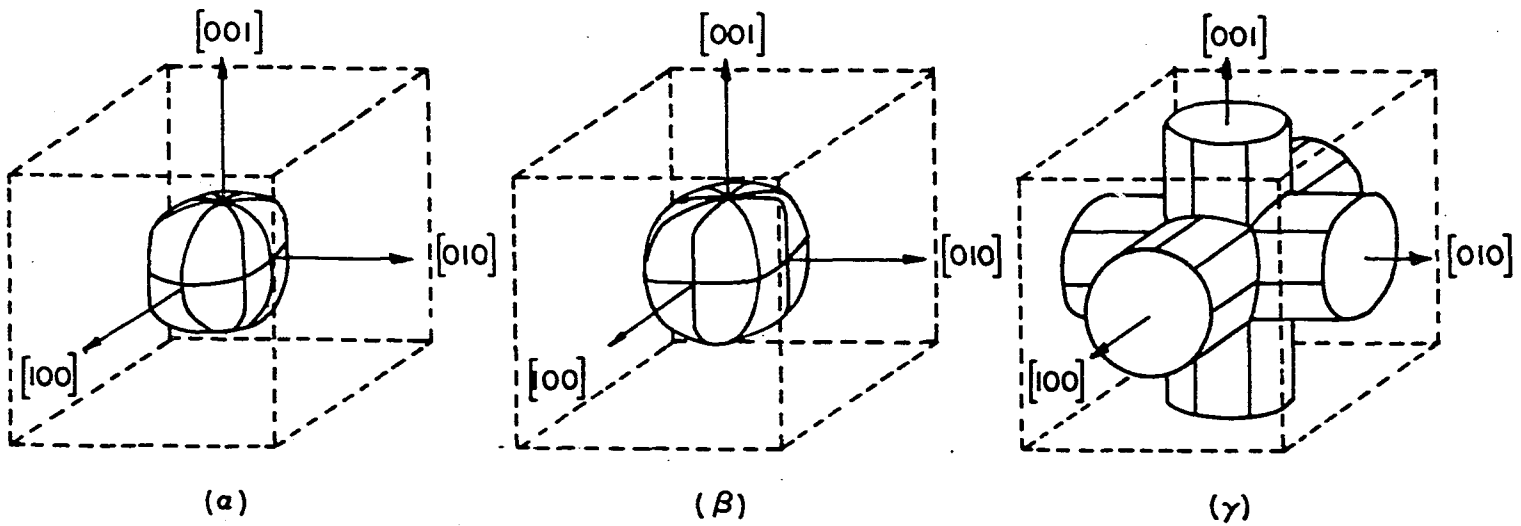

Figure 13. Sketches in three-dimensions of the α, β, and γ sheets of the $NaWO_3$ Fermi surface, after Mattheiss

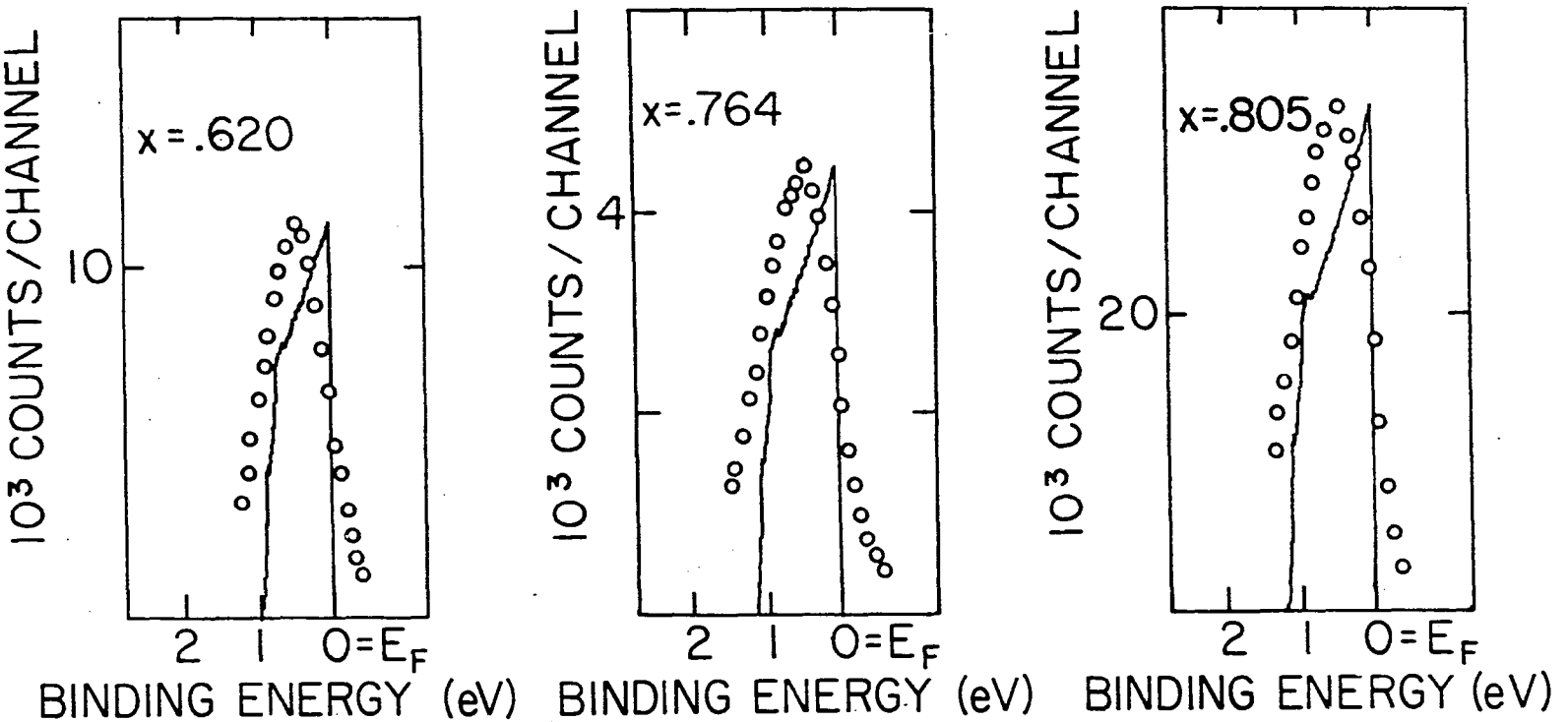

Figure 14. Comparison of photoemission data for the conduction band of Na_xWO_3 with the calculated density of states up to the Fermi energy. The experimental and theoretical Fermi energies have been matched, and the calculated density of states has been scaled to fit the maximum in the data

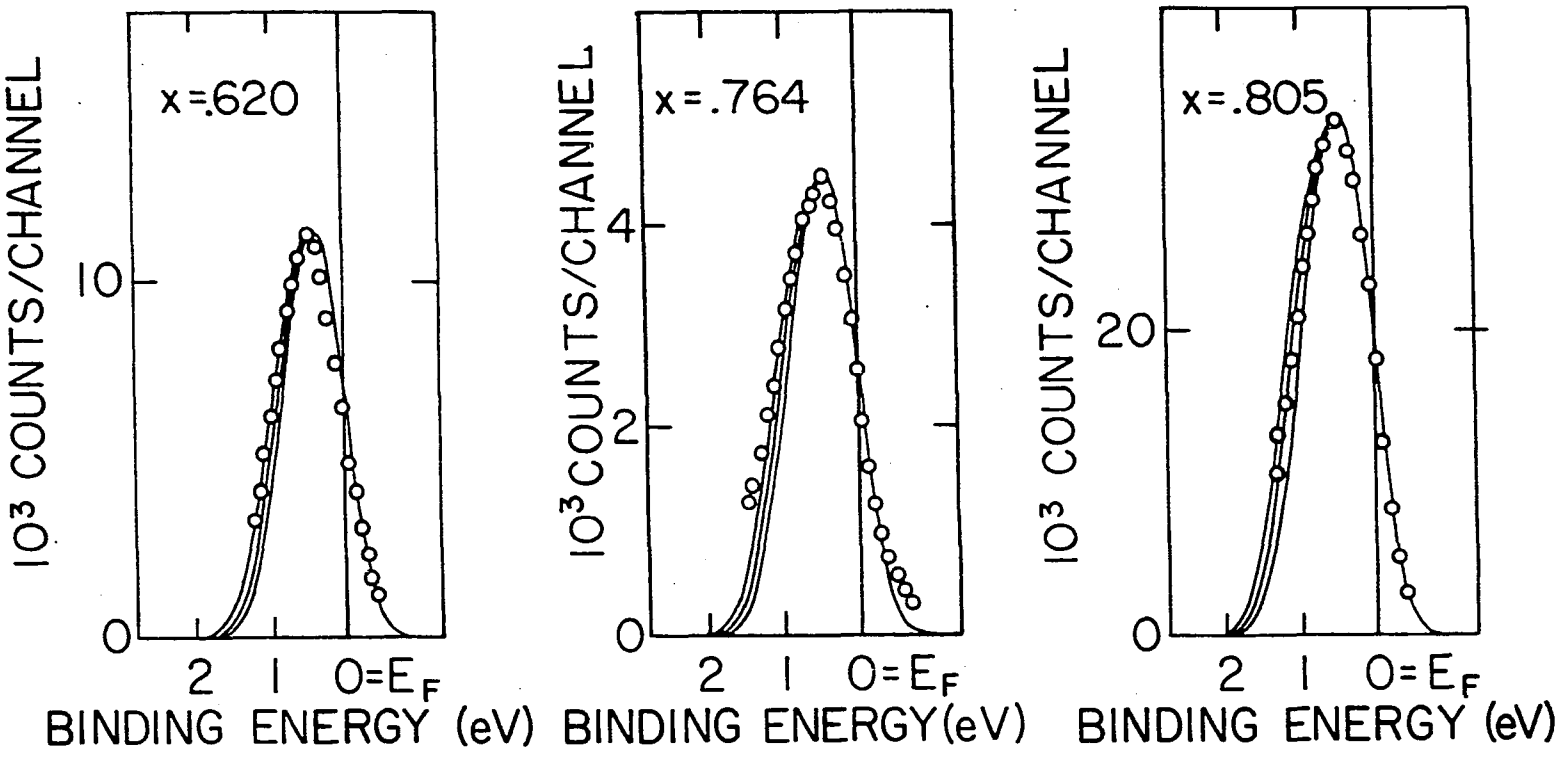

Figure 15. Comparison of photoemission data for the conduction band of Na_xWO_3 with the calculated density of states as in Figure 14, but smoothed by a 0.55 eV gaussian, the resolution function of the spectrometer used to obtain the XPS data. The three curves shown are, from right to left, linear expansions of the calculated density of states of 0, 10, and 20 percent

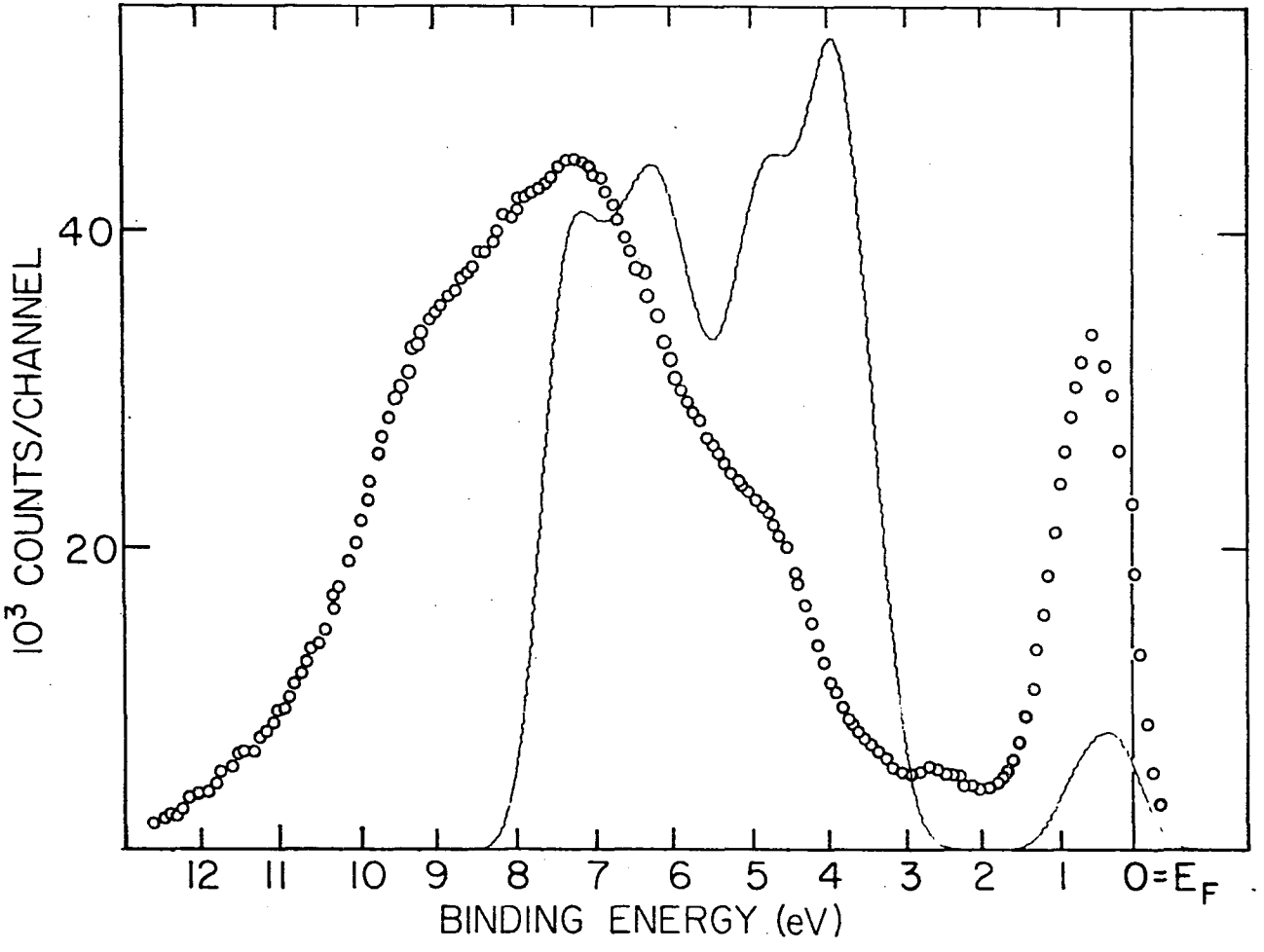

Figure 16. Comparison of photoemission data with the density of states calculated for $NaWO_3$. The experimental and theoretical Fermi energies have been matched, and the calculated density of states has been scaled so that the peak at 6.3 eV fits the maximum in the XPS data for the valence band

percent broader than calculated. Figure 16 shows that the photoemission spectrum does not simply reproduce the density of states; the large peak at the top of the valence band in the density of states is absent in the photoemission results. This will be the subject of further comment after the orbital contributions to the density of states have been presented.

Recent inelastic neutron scattering measurements on single crystals of cubic Na_xWO_3 (104) confirm the two-dimensional character of the Fermi surface and the validity of the rigid band model for these bronzes. The data shown in Figure 17 exhibit a large Kohn anomaly at $(x,\zeta) = (0.56, 0.315)$, $(0.59, 0.345)$, and $(0.83, 0.395)$ in the respective [100] longitudinal acoustic-phonon dispersion curves. Both the position and the shape of this anomaly are in accord with the calculated electronic structure.

Electronic screening affects the longitudinal phonon frequency, $\Omega(\underline{q})$. A simple model (105,106) relates this effect to the electron-phonon interaction $W(\underline{q})$, the electron-electron interaction $V(\underline{q})$, and the susceptibility $\chi(\underline{q})$:

$$\omega^2(\underline{q}) = \Omega^2(\underline{q}) - \frac{W^2(\underline{q})}{V(\underline{q}) + 1/\chi(\underline{q})} .$$

A Kohn anomaly is a sharp feature in a dispersion relation produced by the singular behavior of $\chi(\underline{q})$. The dependence of χ on $\underline{q}$ is

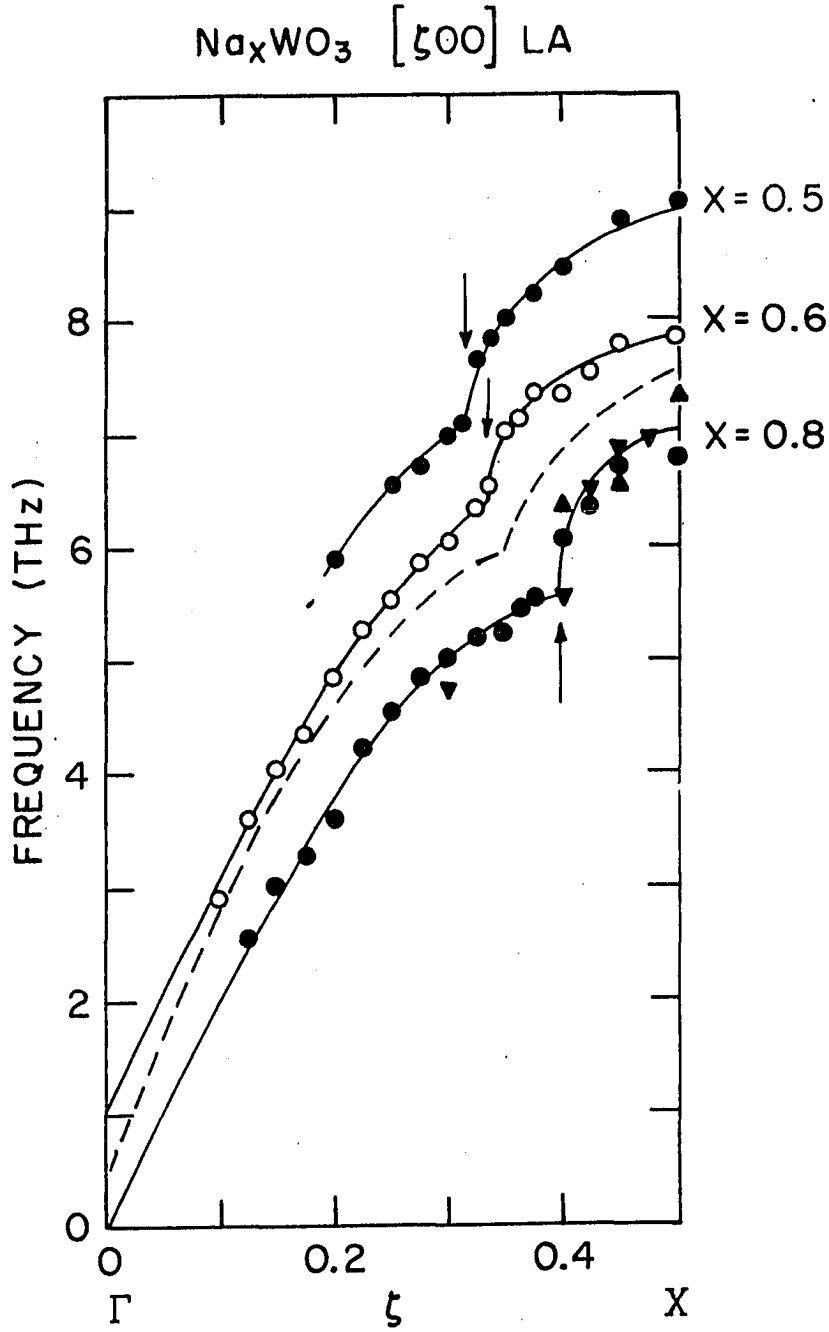

Figure 17. Longitudinal acoustic-phonon dispersion curves for Na_xWO_3 along the [100] direction. Arrows indicate the positions of the Kohn anomalies. The simple model mentioned in the text gives the dashed curve. The curves for x = 0.56 and 0.59 have been displaced upward by 2THz and 1THz, respectively (1THz = 4.14 meV)

$$\chi(\underline{q}) = \sum_{\underline{k}} \frac{f(\underline{k}) - f(\underline{k}+\underline{q})}{E(\underline{k}+\underline{q}) - E(\underline{k})} ,$$

where $f(\underline{k})$ is the Fermi function. $\chi(\underline{q})$ is singular whenever $\underline{q}$ spans a significant piece of the Fermi surface.

The results of numerical calculations of the $\underline{q}$-dependent susceptibility of Na_xWO_3 (104) are presented in Figure 18. The geometry of the Fermi surface largely determines the $\underline{q}$-dependence of χ (107). For a cylindrical Fermi surface, with $\underline{q}$ perpendicular to the cylinder axis, $\chi(\underline{q})$ can be evaluated analytically. Such a χ, for a cylinder diameter $\zeta = 0.35$, is labeled "analytic" in Figure 18. The two-dimensional character of the Fermi surface derived from the KKR band structure is evident in the similarity of the analytical and numerical curves.

The $\underline{q}$ at which the calculated $\chi(\underline{q})$ exhibits a dramatic discontinuity in slope is the $\underline{q}$ at which the Kohn anomaly occurs. This $\underline{q}$ equals the X-Γ-X Fermi surface caliper. By using the rigid band model, the theoretical calipers were found to be $\underline{q} = 0.332$, 0.342, and 0.404 for $x = 0.56$, 0.59, and 0.83, respectively. These values are in good agreement with the observed positions of the Kohn anomalies, demonstrating the applicability of the rigid band model to cubic sodium tungsten bronze.

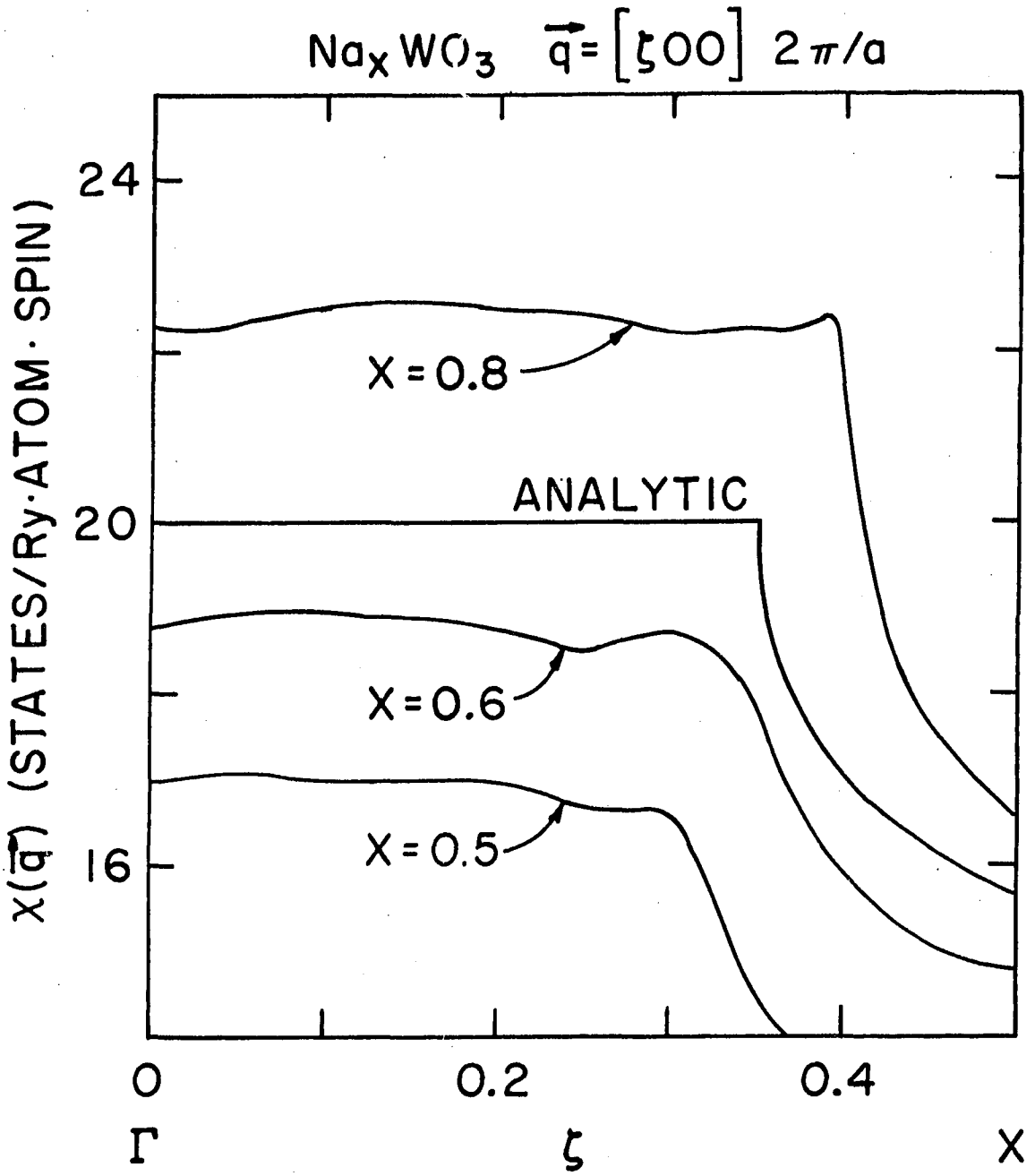

Figure 18. Numerically calculated q-dependent susceptibility of Na_xWO_3 along the [100] direction for three x values. The curve labeled "analytic" is the exact susceptibility for q perpendicular to the axis of a cylinder of diameter $\zeta = 0.35$. A constant (q-independent) term has been added to account for contributions from other bands

To determine the character of the electronic states that form the valence and lowest conduction bands, the wavefunctions of these states were studied. Each wavefunction was normalized accurately by following the ingenious procedure of Janak et al. (108) that requires no knowledge of a crystalline wavefunction outside the muffin-tin spheres. From each wavefunction's coefficients and radial parts was calculated the fraction of an electron inside each muffin-tin sphere which has s, p, or d character. The fractions for each orbital character inside each sphere are contributions to the density of states (DOS), and determine an orbital DOS. The orbital densities calculated for $NaWO_3$ are shown in Figure 19 along with their sum (curve b) and the total DOS (curve a). The difference in area between the sum and total equals the number of electrons outside the muffin-tin spheres. To include these electrons would require knowing the interstitial part of each wavefunction, partitioning this part in some more or less arbitrary fashion among the atomic sites, and then expanding the part assigned each site in its many angular momentum components.

The technique (109) used to construct the curves in Figure 19 is discussed fully in the Appendix. There is remarkable agreement between the sum of the orbital contributions and the total DOS. Other attributes are: (1) that most of the structure present in each orbital DOS also appears

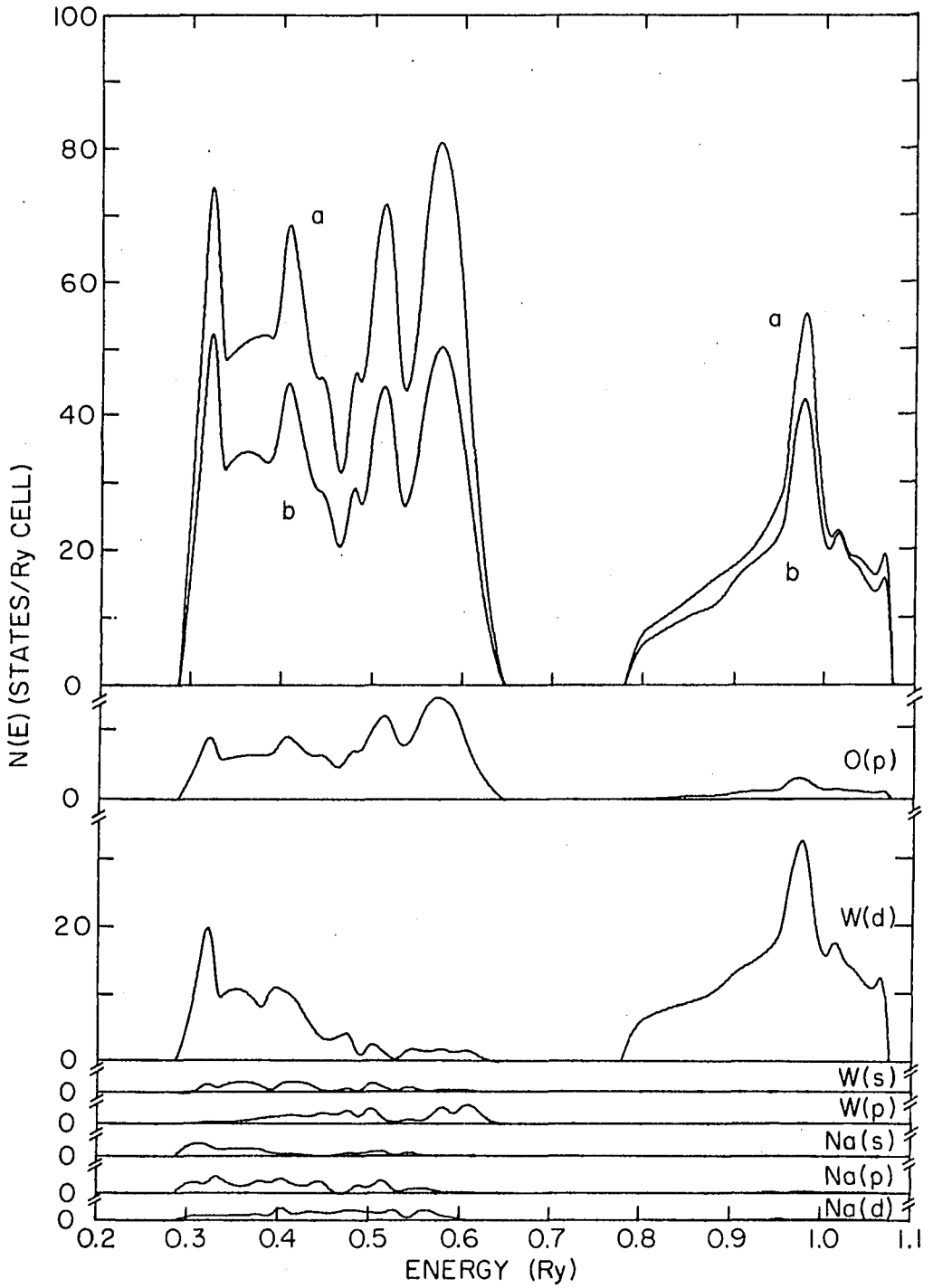

Figure 19. Orbital densities of states for $NaWO_3$ together with their sum (curve b) and the total density of states (curve a)

in the total DOS; (2) that structure not evident in the total DOS is small and often appears in more than one orbital DOS; (3) that spurious structure is scarce, small, and stands out in a comparison against the best available estimate of the total DOS (Figure 9); and (4) that these are smooth curves, not histograms with either low resolution or large fluctuations.

The orbital densities of states presented here make plain the covalent nature of the chemical bonding in the tungsten bronzes. In the valence band, particularly in its lower half, the W5d orbitals mix strongly with the O2p, while in the conduction band, the O2p orbitals mix appreciably with the W5d. The predominance of p and d character on all the atomic sites leads to a very nonspherical distribution of the valence electron charge density about each of them, and suggests the importance of directional bonding in $NaWO_3$, especially between W and O. The Na contribution to the conduction band DOS is found to be negligible, a result which is consistent with nuclear resonance measurements (33, 58-60), XPS core-level line-shape analysis (103), observation of de Haas-van Alphen oscillations in the analogous compound $Na_{0.93}MoO_3$ (110,10), and observation of Na_xWO_3 transport properties at high x values like those of the isoelectronic compound ReO_3. The presence of Na contributions everywhere in the valence bands suggests that it is through these states

that Na affects chemical bonding and produces crystallographic changes (24,35) with changes of its concentration.

The difference mentioned earlier between the photoemission spectrum and the density of states of Na_xWO_3 has also been of concern in the study of ReO_3 (111). This difference in the ReO_3 results has been interpreted as due to a very small contribution to the photoemission spectrum made by the O2p electrons. Gratifying agreement was obtained by comparing the XPS data with just the Re5d contribution. The data also suggested a surprisingly large value for the ratio of the 5d and 2p photoelectron cross sections. By contrast, a comparison of the Na_xWO_3 photoemission results for the valence band with just the W5d contribution presented in Figure 19 provides no better agreement than does comparison with the total DOS. Furthermore, the $NaWO_3$ results suggest a smaller cross section ratio. The W5d contribution alone, however, does provide much better relative magnitudes for the valence and conduction bands of the XPS data than does the total DOS.

BIBLIOGRAPHY

1. J. B. Goodenough, Progr. Solid State Chem. 5, 145 (1971).
2. J. M. Keller, J. Chem. Phys. 33, 232 (1960).
3. A. R. Mackintosh, J. Chem. Phys. 38, 1991 (1963).
4. M. J. Sienko, Adv. Chem. Ser. 39, 294 (1963).
5. R. Fuchs, J. Chem. Phys. 42, 3781 (1965).
6. J. B. Goodenough, Bull. Soc. Chim. (France) 4, 1200 (1965).
7. J. M. Honig, J. O. Dimmock, and W. H. Kleiner, J. Chem. Phys. 50, 5232 (1969).
8. L. F. Mattheiss, Phys. Rev. 181, 987 (1969).
9. L. F. Mattheiss, Phys. Rev. B 2, 3918 (1970).
10. L. F. Mattheiss, Phys. Rev. B 6, 4718 (1972).
11. P. G. Dickens and M. S. Whittingham, Quart. Rev. Chem. Soc. (London) 22, 30 (1968).
12. P. Hagenmuller, Progr. Solid State Chem. 5, 71 (1971).
13. F. Woehler, Ann. Physik Chem. 2, 345 (1824).
14. F. Woehler, Ann. Chim. Phys. 29, 43 (1825).
15. G. Haegg, Nature 135, 874 (1935).
16. G. Haegg, Z. Physik Chem. B29, 192 (1935).
17. J. Phillip and P. Schwebel, Berichte 12, 2234 (1879).
18. H. R. Shanks, J. Cryst. Growth 13/14, 433 (1972).
19. G. Haegg and A. Magneli, Rev. Pure Appl. Chem. (Australia) 4, 235 (1954).
20. P. J. Wiseman and P. G. Dickens, J. Solid State Chem. 17, 91 (1976).
21. M. Atoji and R. E. Rundle, J. Chem. Phys. 32, 627 (1960).

22. E. O. Brimm, J. C. Brantley, J. H. Lorentz, and M. H. Jellinek, J. Am. Chem. Soc. 73, 5427 (1951).

23. W. F. de Jong, Z. Krist. 81, 314 (1932).

24. F. Takusagawa and R. A. Jacobson, J. Solid State Chem. 18, 163 (1976).

25. A. Magneli, Acta Chem. Scand. 5, 670 (1951).

26. A. Magneli, Arkiv Kemi 1, 269 (1949).

27. W. F. de Jong and H. J. Stek, Z. Krist. 83, 496 (1932).

28. A. S. Ribnick, B. Post, and E. Banks, Adv. Chem. Ser. 39, 246 (1963).

29. G. Andersson, Acta Chem. Scand. 7, 154 (1953).

30. P. A. Lightsey, D. A. Lilienfeld, and D. F. Holcomb, Phys. Rev. B 14, 4730 (1976).

31. W. McNeill and L. E. Conroy, J. Chem. Phys. 36, 87 (1962).

32. F. C. Zumsteg, Phys. Rev. B 14, 1406 (1976).

33. D. P. Tunstall, Phys. Rev. B 11, 2821 (1975).

34. P. A. Lightsey, Phys. Rev. B 8, 3586 (1973).

35. M. A. Wechter, H. R. Shanks, and A. F. Voigt, Inorg. Chem. 7, 845 (1968).

36. B. W. Brown and E. Banks, J. Am. Chem. Soc. 76, 963 (1954).

37. G. Bonera, F. Borsa, M. L. Crippa, and A. Rigamonti, Phys. Rev. B 4, 52 (1971).

38. L. D. Muhlstein and G. C. Danielson, Phys. Rev. 158, 825 (1967).

39. T. Hirose, I. Kawano, and M. Niino, J. Phys. Soc. (Japan) 33, 272 (1972).

40. B. I. Crowder and M. J. Sienko, J. Chem. Phys. 38, 1576 (1963).

41. C. Kittel, Introduction to Solid State Physics (Wiley, New York, 1971).

42. L. D. Muhlstein and G. C. Danielson, Phys. Rev. 160, 562 (1967).

43. H. R. Shanks, P. H. Sidles, and G. C. Danielson, Adv. Chem. Ser. 39, 237 (1963).

44. L. D. Ellerbeck, H. R. Shanks, P. H. Sidles, and G. C. Danielson, J. Chem. Phys. 35, 298 (1961).

45. W. R. Gardner and G. C. Danielson, Phys. Rev. 93, 46 (1954).

46. B. W. Brown and E. Banks, Phys. Rev. 84, 609 (1951).

47. E. J. Huibregtse, D. B. Barker, and G. C. Danielson, Phys. Rev. 84, 142 (1951).

48. M. E. Straumanis and W. Dravnieks, J. Am. Chem. Soc. 71, 683 (1949).

49. I. Webman, J. Jortner, and M. H. Cohen, Phys. Rev. B 13, 713 (1976).

50. A. J. Bevolo, H. R. Shanks, P. H. Sidles, and G. C. Danielson, Phys. Rev. B 9, 3220 (1974).

51. B. C. Gerstein, A. H. Klein, and H. R. Shanks, J. Phys. Chem. Solids 25, 177 (1964).

52. R. W. Vest, M. Griffel, and J. F. Smith, J. Chem. Phys. 28, 293 (1958).

53. J. D. Greiner, H. R. Shanks, and D. C. Wallace, J. Chem. Phys. 36, 772 (1962).

54. M. J. Sienko, J. Am. Chem. Soc. 81, 5556 (1959).

55. F. Kupka and M. J. Sienko, J. Chem. Phys. 18, 1296 (1950).

56. P. M. Stubbin and D. P. Mellor, J. Proc. Roy. Soc. N. S. Wales 82, 225 (1948).

57. W. D. Knight, Solid State Physics 2, 93 (1956).

58. W. H. Jones, E. A. Garbaty, and R. G. Barnes, J. Chem. Phys. 36, 494 (1962).

59. A. T. Fromhold and A. Narath, Phys. Rev. 136, A487 (1964).

60. A. T. Fromhold and A. Narath, Phys. Rev. 152, 585 (1966).

61. Ch. J. Raub, A. R. Sweedler, M. A. Jensen, S. Broadston, and B. T. Matthias, Phys. Rev. Lett. 13, 746 (1964).

62. H. R. Shanks, Solid State Commun. 15, 753 (1974).

63. K. L. Ngai and R. Silberglitt, Phys. Rev. B 13, 1032 (1976).

64. M. Born and J. R. Oppenheimer, Ann. Phys. 84, 457 (1927).

65. D. R. Hartree, Proc. Camb. Phil. Soc. 24, 89 (1928).

66. D. R. Hartree, Proc. Camb. Phil. Soc. 24, 111 (1928).

67. D. R. Hartree, Proc. Camb. Phil. Soc. 24, 426 (1928).

68. V. Fock, Z. Physik 61, 126 (1930).

69. W. Pauli, Z. Physik 31, 765 (1925).

70. J. O. Dimmock, Solid State Physics 26, 103 (1971).

71. K. Ruedenberg, Rev. Mod. Phys. 34, 326 (1962).

72. D. Pines, Phys. Rev. 92, 626 (1953).

73. J. C. Slater, The Self-consistent Field for Molecules and Solids: Quantum Theory of Molecules and Solids, Vol. 4 (McGraw-Hill, New York, 1974).

74. J. C. Slater, Adv. Quantum Chem. 6, 1 (1972).

75. J. C. Slater, Phys. Rev. 81, 385 (1951).

76. E. Wigner and F. Seitz, Phys. Rev. 43, 804 (1933).

77. E. Wigner and F. Seitz, Phys. Rev. 46, 509 (1934).

78. E. Wigner, Phys. Rev. 46, 1002 (1934).

79. J. Korringa, Physica 13, 392 (1947).

80. W. Kohn and N. Rostoker, Phys. Rev. 94, 1111 (1954).

81. B. Segall, Phys. Rev. 105, 108 (1957).

82. F. S. Ham and B. Segall, Phys. Rev. 124, 1786 (1961).

83. B. Segall and F. S. Ham, Methods Comput. Phys. 8, 251 (1968).

84. H. W. Myron, Ph.D. Thesis, Iowa State University, 1972 (unpublished).

85. M. Becker, The Principles and Applications of Variational Methods (The M.I.T. Press, Cambridge, Massachusetts, 1964).

86. S. T. Epstein, The Variational Method in Quantum Chemistry (Academic Press, New York, 1974).

87. J. M. Ziman, Solid State Physics 26, 1 (1971).

88. J. C. Slater, Quantum Theory of Molecules and Solids, Vol. 2 (McGraw-Hill, New York, 1965).

89. F. Herman and S. Skillman, Atomic Structure Calculations (Prentice Hall, Englewood Cliffs, New Jersey, 1963).

90. L. F. Mattheiss, Phys. Rev. 133, A1399 (1964).

91. J. Keller, J. Phys. C 4, L85 (1971).

92. J. M. Ziman, J. Phys. (Paris) 33, C3-209 (1972).

93. E. C. Snow and J. T. Waber, Phys. Rev. 157, 570 (1967).

94. J. W. D. Connolly, Phys. Rev. 159, 415 (1967).

95. D. A. Papaconstantopoulos, J. R. Anderson, and J. W. McCaffrey, Phys. Rev. B 5, 1214 (1972).

96. J. R. Anderson, D. A. Papaconstantopoulos, J. W. McCaffrey, and J. E. Schirber, Phys. Rev. B 7, 5115 (1973).

97. P. F. Walch and D. E. Ellis, Phys. Rev. B 8, 5920 (1973).

98. H. W. Myron and A. J. Freeman, Phys. Rev. B 9, 481 (1974).

99. V. L. Moruzzi, A. R. Williams, and J. F. Janak, Phys. Rev. B 9, 3316 (1974).

100. O. Jepsen and O. K. Andersen, Solid State Commun. 9, 1763 (1971).

101. G. Lehman and M. Taut, Phys. Stat. Sol. 54, 469 (1972).

102. T. Wolfram, Phys. Rev. Lett. 29, 1383 (1972).

103. M. Campagna, G. K. Wertheim, H. R. Shanks, F. Zumsteg, and E. Banks, Phys. Rev. Lett. 34, 738 (1975).

104. W. A. Kamitakahara, B. N. Harmon, J. G. Traylor, L. Kopp, and H. R. Shanks, Phys. Rev. Lett. 36, 1393 (1976).

105. D. Pines, Elementary Excitations in Solids (Benjamin, New York, 1964).

106. S. K. Sinha and B. N. Harmon, Phys. Rev. Lett. 35, 1515 (1975).

107. W. E. Evenson and S. H. Liu, Phys. Rev. 178, 783 (1969).

108. J. F. Janak, A. R. Williams, and V. L. Moruzzi, Phys. Rev. B 11, 1522 (1975).

109. L. Kopp, Department of Chemistry, Iowa State University, (to be published).

110. S. M. Marcus and T. A. Bither, Phys. Rev. Lett. 23, 1381 (1969).

111. G. K. Wertheim, L. F. Mattheiss, M. Campagna, and T. P. Pearsall, Phys. Rev. Lett. 32, 997 (1974).

ACKNOWLEDGMENTS

The scant attention paid in the West to obligations to those people, past and present, who have affected our lives for the better, stands in sharp contrast to the strong sense of indebtedness to the world felt in the East. As a tribute to Professors Bernard Gerstein and Samuel Liu, my mentors throughout my research, this thesis, an outgrowth of their constant confidence and concern for my success, can be no more than a token.

Without the expertise of Dr. Bruce Harmon, whose willingness to be of help exceeded what one has any right to expect, this work could not have been carried as far.